UPPSALA
UNIVERSITET

UPTEC STS 19 045
Examensarbete 30 hp
Oktober 2019

Vibration analysis of a fast response brushless excitation system

Emma Pålsson

UPPSALA
UNIVERSITET

Teknisk- naturvetenskaplig fakultet
UTH-enheten

Besöksadress:
Ångströmlaboratoriet
Lägerhyddsvägen 1
Hus 4, Plan 0

Postadress:
Box 536
751 21 Uppsala

Telefon:
018 – 471 30 03

Telefax:
018 – 471 30 00

Hemsida:
http://www.teknat.uu.se/student

Abstract

Vibration analysis of a fast response brushless excitation system

Emma Pålsson

The aim of this study is to measure and analyze vibrations on a fast response brushless exciter (FRBE) at a real hydropower plant and identify vibration origins through frequency analysis. Moreover, the observed vibrations are evaluated in relation to generator vibration standards and estimated tangential eigenfrequencies of the studied FRBE.

It is concluded that the pulsations in the air gap torque, originating from the rotating thyristor bridge rectifier, is the source of the strongest vibrations. Some additional vibration sources are also identified. The requirements of the generator vibration standards are mostly fulfilled and no tangential eigenfrequencies are triggered in the vibration recordings. For further studies it is recommended that alternative control strategies and optimization of the FRBE mechanical design, with respect to its ability to withstand vibrations, should be investigated.

Handledare: Atila Pardini
Ämnesgranskare: Urban Lundin
Examinator: Elísabet Andrésdóttir
ISSN: 1650-8319, UPTEC STS 19 045

Populärvetenskaplig sammanfattning

I dagsläget täcker vattenkraften nästan 50 % av Sveriges elbehov. I och med att vattenflöden snabbt kan regleras upp och ner kan vattenkraften på effektivt sätt kompensera för variationer i last. Denna egenskap gör också att vattenkraften spelar en betydande roll för att möjliggöra implementering av förnybar energi från intermittenta källor. Vattenkraften står dock inför stora utmaningar. Den växande efterfrågan på el och den planerade utfasningen av kärnkraften gör att elnätet kommer att belastas hårdare i framtiden. Då är det av yttersta vikt att säkra att vattenkraften kan generera el så kontinuerligt som möjligt.

Ett steg på vägen är att minska underhållsbehovet för vattenkraftsgeneratorer. När statiska matare används för att magnetisera generatorernas fältlindningar uppstår ett frekvent underhållsbehov på grund av koldammsansamlingar. Detta eftersom magnetiseringsströmmen överförs till fältlindningarna genom kolborstar i direktkontakt med släpringar. Problemet med koldamm kan lösas genom att den statiska mataren byts ut mot ett borstlöst, roterande system, utformat på liknande sätt som huvudgeneratorn. De bortslösa matarna har tidigare kritiserats för sin långsamma svarstid, men genom en ändring av styrmekanismen kan de uppgraderas till snabba system som dessutom kräver lite underhåll. Med en sådan uppgradering följer dock nya utmaningar eftersom matarens statorkonstruktion utsätts för starkare vibrationer.

Målet med denna studie är att mäta och analysera vibrationer på en snabbstyrd borstlös matare i ett vattenkraftverk samt att, med hjälp av frekvensanalys, identifiera vibrationernas ursprung. Utöver detta utvärderas de observerade vibrationerna mot vibrationsstandards för generatorer och mot uppskattningar av den studerade matarens tangentiella egenfrekvenser.

Det konstateras att pulsationerna i luftgapsmoment, orsakade av den roterande tyristorbryggan, är källan till de starkaste vibrationerna. Utöver tyristorbryggan identifieras några ytterligare vibrationskällor. Kraven som presenteras i de vibrationsstandard som använts är mestadels uppfyllda och inga tangentiella egenfrekvenser triggas i vibrationsmätningarna. För vidare studier rekommenderas att alternativa kontrollstrategier och optimering av den snabbstyrda matarens mekaniska design, med avseende på dess motståndskraft mot vibrationer, utreds.

Acknowledgements

I would like to thank the generator design department at Voith Hydro AB for their helpfulness and sincere involvement in this project. Moreover, I would like to thank my supervisors Atila Pardini and Olof Torsteinsrud at Voith Hydro AB for giving me the opportunity to go to site. On this remark I also want to thank the hydropower plant owner (anonymous) for the hospitality. Last but not least, I thank my supervisor Urban Lundin at Uppsala University for all the good advice, some of which I should have listened more to.

Abbreviations

AC	Alternating Current
DC	Direct Current
FFT	Fast Fourier Transform
FRBE	Fast Response Brushless Exciter
ISO	International Organization for Standardization
NGTR	Nordic Generator Technical Requirements
RMS	Root Mean Square

Wordlist

Air gap torque
Turning moment of force in the air gap between the rotor and the stator.

AVR
Automatic Voltage Regulator. A feedback loop that controls the field voltage based on measured generator terminal voltage and a reference value.

Ceiling voltage
Maximum generator field voltage available for the excitation system given a certain level of exciter field voltage on the AC-side of the thyristor bridge rectifier.

Controlled rectification
Conversion from AC to DC where the magnitude of the output DC-voltage can be controlled.

Eigenfrequencies
Also called natural frequencies. If a system is exposed to vibrations of these frequencies, it can enter a state of rapidly increasing oscillation.

EMF
Electromotive force. The work done or energy gained per unit of electric charge, expressed in volts.

FCR
Field Current Regulator. A feedback loop that controls the exciter field voltage based on measured exciter field current and a reference exciter field current set point.

Firing angle
Delay angle that is applied to reduce the mean output DC-voltage of a thyristor bridge rectifier. The firing angle specifies when controlled rectification starts, using the phase-crossing at maximum rectification as reference.

Guide vanes
Blades used to control the flow of water through a turbine.

Uncontrolled rectification
Full conversion from AC to DC without possibility to control the magnitude of the output DC-voltage.

PID-regulator
Proportional, integral and derivative regulator.

Reactive power
Parasitic magnetic energy accumulation causing voltage drops and increased losses if not compensated for.

Slots
Trails on exciter rotor and generator stator where armature winding coils are placed.

Table of contents

1. Introduction

Almost 50 % of Sweden's annual power demand is covered by hydropower [1]. Due to its storing ability and high controllability, hydropower enables quick regulation to meet changes in load demand [2]. Hydropower also plays a crucial role in the development of a robust, sustainable power production as it enables integration of intermittent renewable power production. In addition to this, hydropower plants have almost zero CO_2 emissions once constructed [3]. Bearing all this in mind, it is of utter importance that some upcoming challenges are handled.

With increasing power demand and planned nuclear power phase outs come higher constraints on the grid [4]. It is therefore essential that the existing hydropower generation operates as smooth as possible. One step towards ensuring this is by reducing the need for maintenance of hydroelectric synchronous generators. Since carbon dust build-up is a frequent source of generator maintenance, elimination of this problem would significantly reduce hydroelectric generator downtime [5]. Carbon dust build-up is inevitable when using static exciters to magnetize the generator field windings, since the excitation current is transferred to the generator via carbon brushes in physical contact with slip rings. The problem can however be solved by replacing the static exciters with brushless alternatives [6].

Yet, many state-of-the art brushless exciters do have drawbacks in terms of slow response. As a result of this, brushless exciters are not widely used for large hydroelectric generators. But a paradigm shift may be within sight. This since a fast response system can be achieved by replacing the passive diode bridge rectifier, on the rotating side of the brushless exciter, with a controllable thyristor bridge rectifier. Thus, a system with low maintenance and high controllability can be achieved [5]. Such an upgrade does however bring new challenges. When operating at high firing angles, which is desirable in order to achieve a fast response, the thyristor bridge rectifier imposes pulsations in the exciter, and thereby vibrations, that may subject the exciter stator to stress[7] [8].

1.1 Aim

The main aim of this master thesis is to measure and analyze vibration levels on the stator of a fast response brushless exciter (FRBE), identify vibration origins and evaluate the observed vibrations in relation to existing standards and estimated eigenfrequencies. Moreover, the aim is to verify the correlation between vibration severity and firing angle and suggest focal points for mitigating FRBE stator vibrations.

1.2 Scope

This master thesis is part of a FRBE research and development project driven by Voith Hydro AB, where the goal is to accomplish a refined end product.

This paper is a case study, focusing on frequency analysis of vibrations recorded from a FRBE stator at a real hydropower plant. The measures have been done for various load conditions and exciter field current set points. Vibration origins have been identified based on frequency content. The observed vibrations have been evaluated from multiple perspectives using:

- Vibration standards developed for generators
- Estimates of the exciter stator eigenfrequencies

1.3 Disposition

The opening introduction chapter is followed by a background and theory chapter where the FRBE system is described along with its relevant properties. The background and theory chapter also contains information about vibration characteristics and generator vibration standards. In the third chapter, the method for recording and analyzing vibrations is presented. The method chapter is then followed by a data chapter in which the data regarding machine parameters, load conditions etcetera is found. The fifth chapter is devoted to results and analysis and the conclusions of the study are presented in chapter six.

2. Background and theory

This chapter contains the relevant background and theory for the project. It is introduced with a brief overview of synchronous generators and exciters. After this, a more thorough description of the FRBE system and its properties is presented. This is followed by a description of the expected frequency content of exciter stator vibrations, generator vibration standards and other criteria used to evaluate vibration severity. Finally, some of the findings from previous work on FRBE stator vibrations are summarized.

2.1 Synchronous generators and exciters

A cross section of a synchronous generator is illustrated in Figure 1. Synchronous generators primarily account for the conversion of mechanical energy into electrical energy and then for supplying power to the grid.

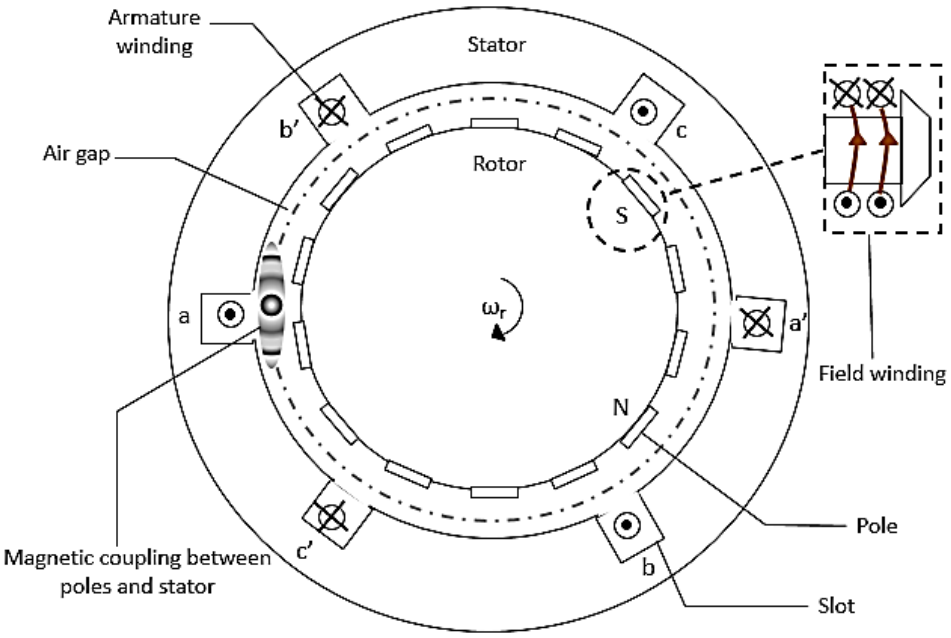

Figure 1. Cross section of a synchronous generator, as seen from above.

When the field windings of the iron rotor is excited with DC-current during rotation, a rotating magnetic field arises in the air gap separating the rotor from the stator. This rotating magnetic field then induces a time-varying EMF in the three-phase winding of the stator armature [2]. The excitation of the rotor field windings is provided by an exciter. In addition to this, the exciter plays a crucial role in maintaining reactive power balance as it enables the generator to deliver and absorb reactive power in accordance with the state of the grid, thus preventing voltage drops at the generator terminals [9].

Exciters can be either static or rotating. The static exciter feeds DC-current to the generator rotor via rotating slip rings using carbon brushes. As for the rotating brushless exciter, the exciter is itself a small outer pole generator attached to the main generator shaft. The brushless exciter induces AC-current which are then rectified to DC before exciting the synchronous generator rotor windings [10] [11]. An illustration of a brushless exciter, mounted on the main generator shaft, can be seen in Figure 2.

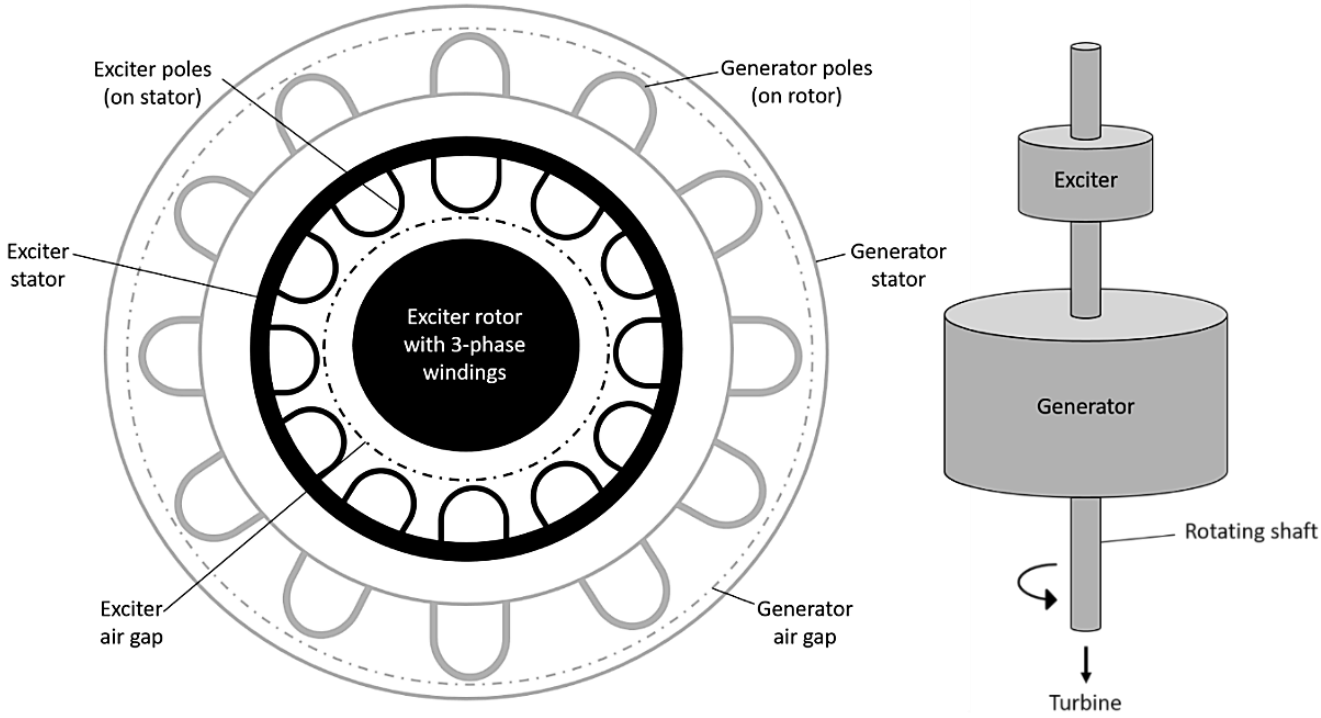

Figure 2 a) Illustration of a brushless exciter mounted on the main generator shaft, as seen from above. b) As seen from in front.

2.2 FRBE system properties

The FRBE is in essence a small generator with its poles located on the stator instead of on the rotor. It derives its own excitation either from a permanent magnet or from an auxiliary source, often a local low-voltage AC or DC power supply. In this thesis focus is on the latter and hence the permanent magnet exciter will not be further explained.

A schematic illustration of the FRBE system can be seen in Figure 3. The power supply feeds AC-voltage to a stationary rectifier that converts it to DC. The corresponding DC-current, called the exciter field current, magnetizes the exciter stator windings. The resulting rotating magnetic field in turn induces AC-voltage in the exciter rotor windings. Thereafter, the rotating thyristor bridge rectifier, mounted on the main generator shaft, rectifies the exciter output AC-voltage to DC before the rotor windings of the synchronous generator are finally excited. The DC-current exciting the generator rotor windings is called the generator field current [10] [12].

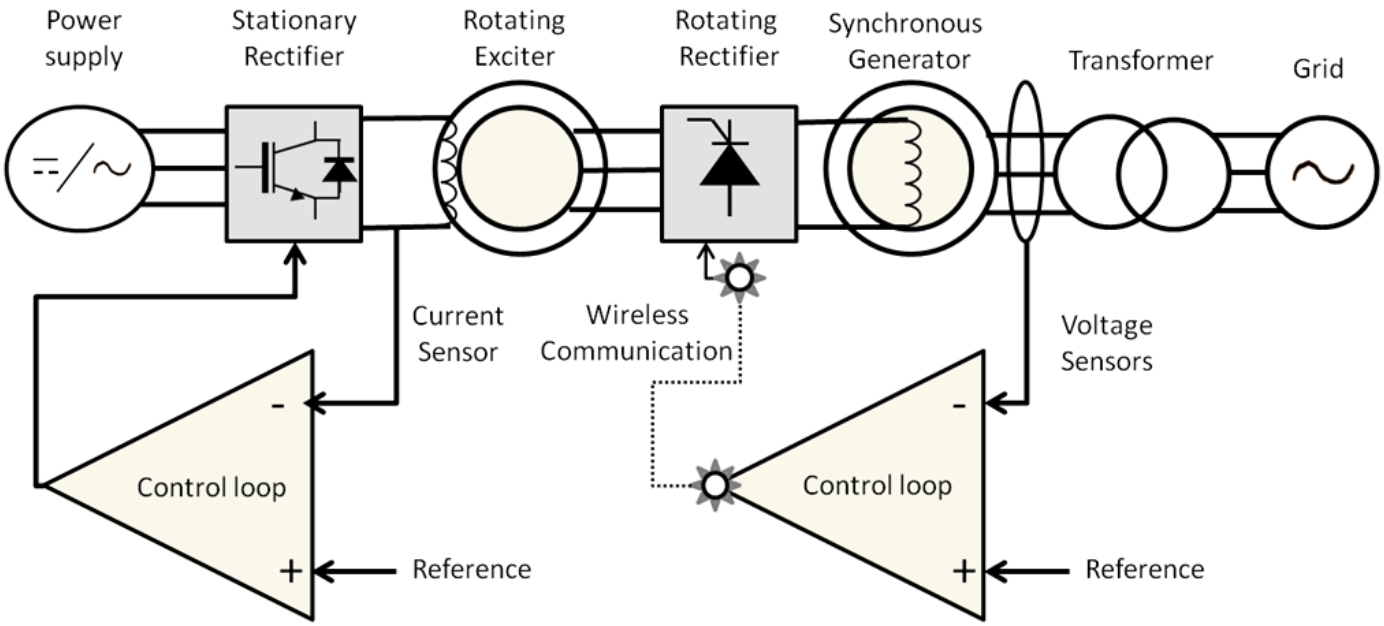

Figure 3. Schematic illustration of the FRBE system.

2.2.1 Controlled rectification

The FRBE system has a fast response time compared to the conventional brushless excitation system since it utilizes controllable rectifiers also on the rotating side. This enables direct control of the generator rotor circuitry in addition to the exciter stator field windings. The conventional brushless excitation system instead uses a non-controllable diode bridge rectifier on the rotating side [7].

Thyristors are triggered into conduction via pulses that are supplied to their gates by a firing card. A different thyristor is triggered every 60 electrical degrees and is governed by the phase-to-phase voltage crossing and a controllable delay called firing angle. A firing angle of 15 degrees means that the firing card triggers the thyristors into conduction 15 degrees after the phase-to-phase voltage crossing [11]. Conduction will then continue until the current is zero or until the next thyristor starts conducting. Figure 4 and Figure 5 illustrate the concepts of uncontrolled and controlled rectification.

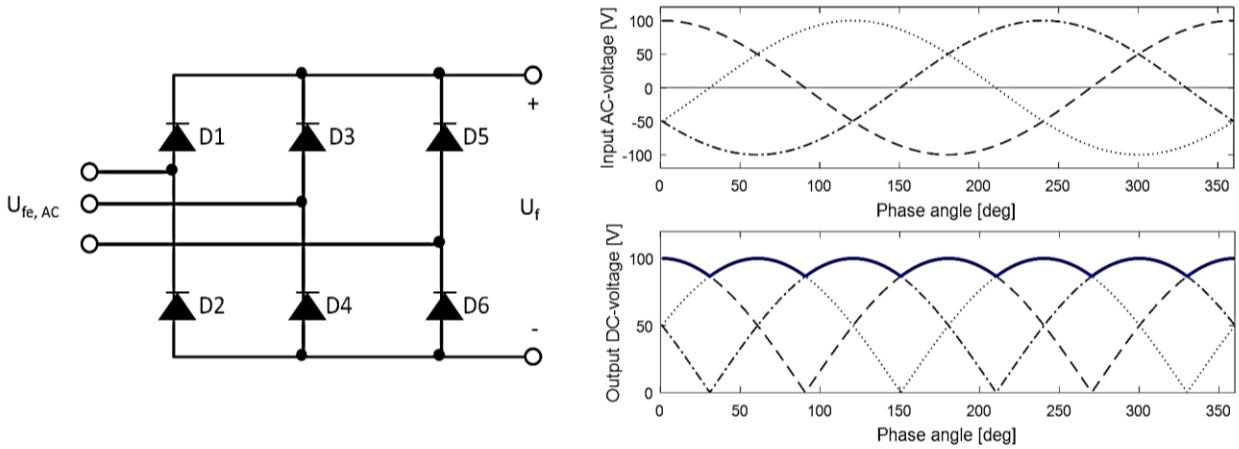

Figure 4 a) Circuit representation of a three-phase diode bridge rectifier. b) Uncontrolled rectification. The bold curve shows the resulting DC-voltage.

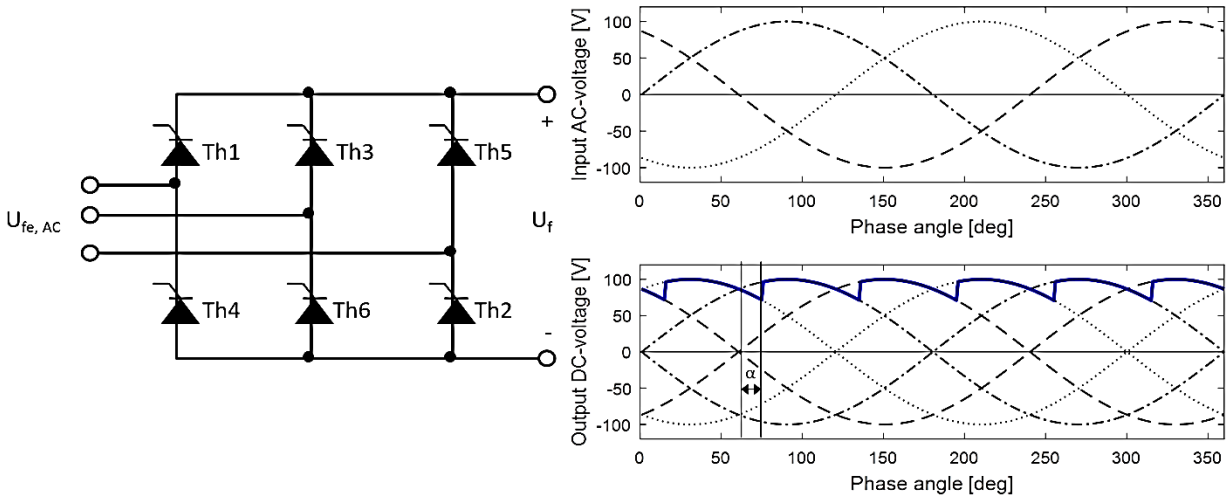

Figure 5 a) Circuit representation of a three-phase thyristor bridge rectifier. b) Controlled rectification with a 15° firing angle. The bold curve shows the resulting DC-voltage.

As can be seen in Figure 4 and Figure 5, the firing angle α governs the magnitude of the mean output DC-voltage of the thyristor bridge rectifier. Hence, by adjusting the firing angle for the rotating thyristor bridge rectifier of a FRBE system, the generator field voltage can be controlled [5]. If the RMS AC exciter field voltage and the generator field voltage are known, the firing angle of the rotating thyristor bridge rectifier can be estimated using Eq.1

$$\alpha = \cos^{-1}\left(\frac{U_f}{1.35 \cdot U_{fe,AC}}\right) \quad \text{[deg]} \qquad \text{(Eq.1)}$$

where $U_{fe,AC}$ is the exciter rotor voltage and U_f is the generator field voltage.

2.2.2 Ceiling voltage

For power system stability, it is positive to operate the FRBE system with a high exciter field voltage compared to the required generator field voltage level for the specific load conditions. This excess of exciter field voltage enables rapid increase of the generator field voltage. The maximum generator field voltage available for the excitation system at a given exciter field voltage level is called the ceiling voltage. In turn, the ratio between the ceiling voltage and the generator field voltage is called the ceiling voltage factor [5].

To maintain the possibility to rapidly increase the generator field voltage, the ceiling voltage must be significantly higher than the generator field voltage. This in turn means that the magnitude of the exciter rotor voltage on the AC-side of the rotating thyristor bridge rectifier needs to be considerably higher than the magnitude of the generator field voltage on the DC-side. Thus, in order to achieve a high ceiling voltage factor, the rotating thyristor bridge rectifier is required to operate at high firing angles [5].

2.2.3 Control loops

The firing card control signal, governing at what point the thyristors start conducting, comes from a controller. Essentially, the controller contains control loops, mainly with a PID-structure. The Automatic Voltage Regulator (AVR), illustrated in Figure 6, is used for automatic control of the generator terminal voltage, U_g. Measurements of the generator terminal voltage are compared in a feedback loop to a desired reference value. The regulator corrects the error by sending a control signal to the firing card through wireless communication. The firing card then adjusts the firing angle of the thyristor bridge rectifier so that the intended outcome is achieved. In addition to keeping the generator terminal voltage stable, the AVR control mode also includes a plethora of limiter functions that aim to maintain the generator within its defined region of safe operation [13].

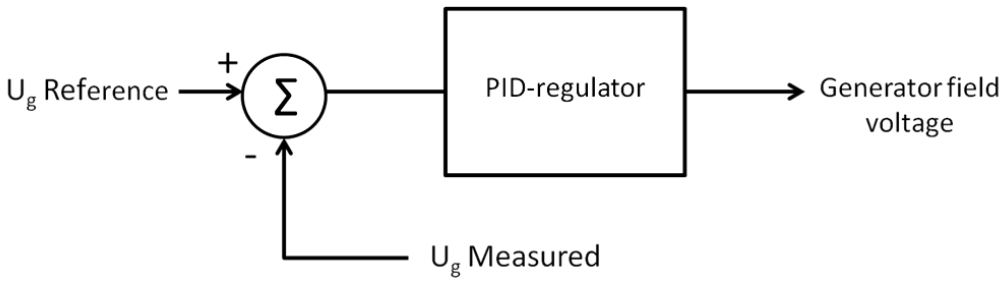

Figure 6. Schematic representation of the AVR.

In the studied FRBE system, the exciter is controlled parallel to the generator (see Figure 3) using a Field Current Regulator (FCR). The FCR, shown in Figure 7, takes an exciter field current set point as reference. Actual measurements of the exciter field current, I_{fe}, are then compared to this set point in a feedback loop [13].

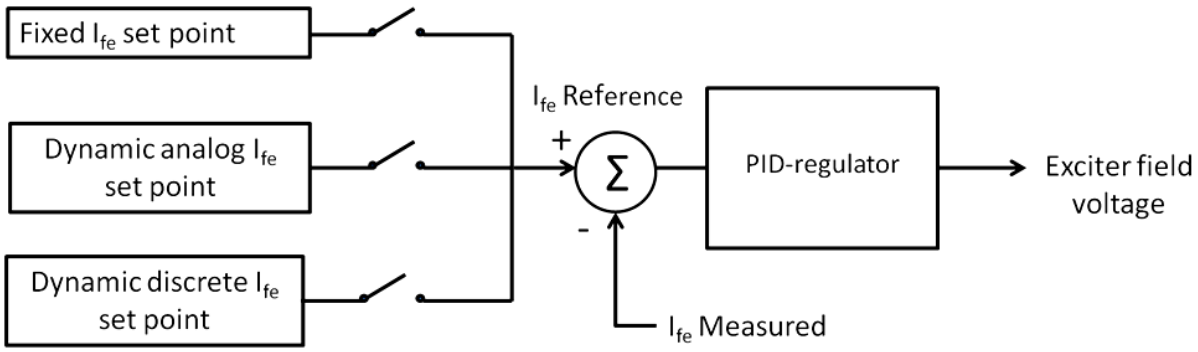

Figure 7. Schematic representation of the FCR and the exciter field current set point options.

As is seen in Figure 7, there are three options when selecting the exciter field current set point; fixed, dynamic analog and dynamic discrete. When the exciter field voltage is controlled based on a fixed exciter field current set point, the exciter field current is kept at a fixed level and does not change with changing conditions. Thus, if the operator sets the fixed exciter field current set point to 1.8, the exciter field current will remain at a level of 1.8 times its no load base value. Fixed exciter field current set points require manual control and are primarily applied during no load testing.

Choosing instead to use a dynamic analog exciter field current set point, the FCR will take into account the generator field current when controlling the exciter field voltage. A dynamic analog exciter field current set point of 1.3 means that the exciter field current level is dynamically changed by the actual generator field current level so that the exciter field voltage matches the varying load demands whilst the ceiling voltage availability is kept. For the dynamic discrete exciter field current set point, the FCR considers active power load levels when controlling the exciter field voltage. However, as the dynamic discrete set point option was not available during the tests conducted in this work, the dynamic analog exciter field current set point is referred to as dynamic exciter field current set point throughout this paper. Moreover, fixed and dynamic analog exciter field current set points are denoted FF_sp and FD_sp in graph and table indexes.

2.2.4 Torque pulsations

For hydropower plants it is common that the requirements on ceiling voltage availability calls for application of high firing angles. On the one hand, high firing angles lead to a faster responding system. On the other hand, high firing angles also lead to more ripple in the output DC-voltage of the thyristor bridge rectifier and thereby to more disturbances due to harmonic currents.

The voltage and current supplied to the exciter governs the exciter air gap torque, and thereby the rotational power of the exciter. The presence of harmonic currents and voltage ripples lead pulsations of the exciter air gap torque, resulting in the exciter rotor attempting to rotate the exciter stator. Thus, as the pulsating air gap torque subjects the exciter stator to stress, high firing angles are undesirable during steady state operation [7] [8] [14].

The pulsations in the air gap torque occur also for the conventional brushless exciters, though rather small compared to those of an FRBE [5]. For an exciter using a three-phase, six-pulse thyristor bridge rectifier, analytical models and simulations indicate that the total harmonic distortion of the torque waveform increases exponentially with higher firing angles [15]. Previous on-site measurements of FRBE air gap torque pulsations confirm this behavior [16]. Also the torque pulsations appear to become more severe if the generator field current is high [14].

2.3 Vibrations on the exciter stator

As mentioned before, FRBE systems are facing a challenge as the exciter stators are subjected to higher vibration levels compared to those of the conventional brushless excitation systems. Below follows an overview over some known vibration sources and features. In addition to this, requirements regarding acceptable vibration levels are presented along with some mitigation strategies proposed in previous work on the subject.

2.3.1 Radial and tangential forces

When in rotation, the FRBE rotor is subjected to radial and tangential forces, as illustrated in Figure 8. The radial forces work outwards along the exciter radius and they arise mainly from rotation due to the mass of the machine. The tangential forces are orthogonal to the radial forces. They govern the power output of the exciter and originate from the magnetic coupling between its stator and rotor. When using a thyristor bridge rectifier, tangential forces can also occur as a consequence of brief short circuits from the firing of the thyristors. Moreover, the exciter is subjected to tangential forces due to torque pulsations from rectification [6] [17].

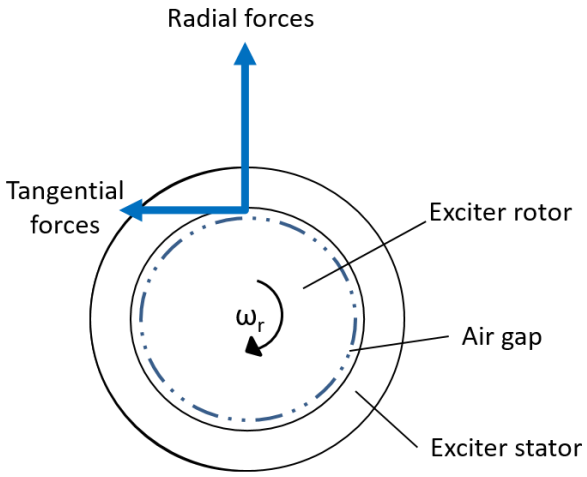

Figure 8. Radial and tangential forces on exciter rotor as seen from above.

Forces on the exciter rotor are transmitted onto the stator and result in vibrations, both radial and tangential. If too severe, the vibrations might damage the stator. The rotor on the other hand, has greater ability to tolerate the impact of these forces due to its large mass [17].

2.3.2 Electrical and mechanical frequency content

By measuring vibrations on the FRBE stator, more information can be gained regarding the exciting force harmonics involved. Analysis of the frequency content of the measured vibrations can then be applied to identify their origins.

For a FRBE with the speed n_s revolutions per minute and p_n poles, its electrical frequency f_e can be calculated using Eq.2, rewritten as Eq.3.

$$n_s = \frac{120 \cdot f_e}{p_n} \quad \text{[rpm]} \quad \text{(Eq.2)}$$

$$f_e = \frac{n_s \cdot p_n}{120} \quad \text{[Hz]} \quad \text{(Eq.3)}$$

The frequencies (f_n) of the harmonics originating from six-pulse rectification are then found using Eq.4. These harmonics will have frequencies of 6, 12, 18, 24… times the electrical frequency of the exciter.

$$f_n = 6n \cdot f_e \quad \text{[Hz]} \quad \text{(Eq.4)}$$

As the order n increases, the magnitude of the harmonics decreases rapidly. Hence, high order harmonics can often be neglected. The main impact from the harmonic disturbances comes from the first order harmonic ($n = 1$).

In addition to the electrical frequencies, there are vibrations on the FRBE that arise from mechanical sources. As previously mentioned, rotation subjects the exciter stator to forces which may cause vibrations. Some mechanical frequencies are expected to be

found in the spectra of the measured vibrations while other may indicate fault or wear [17].

One of the mechanical frequencies expected to dominate the contribution to the vibrations is the rotational frequency f_{rot} [17]. This frequency can be calculated as shown in Eq.5.

$$f_{rot} = \frac{n_s}{60} \quad [\text{Hz}] \quad \text{(Eq.5)}$$

As the exciter and generator are mounted to the same rotating shaft, the rotational frequency is the same for both machines. When inserting Eq.5 into Eq.3, the relation between electrical and mechanical frequency of the exciter is obtained as stated by Eq.6.

$$f_e = f_{rot} \cdot \frac{p_n}{2} \quad [\text{Hz}] \quad \text{(Eq.6)}$$

The rotational frequency is sometimes referred to as 1X. Beside 1X, peaks at integer multiples of the rotational frequency, such as 2X, 3X… are also expected to be found in the spectra of the exciter vibrations. Similar to the electrical harmonics originating from rectification, the amplitude of mechanical harmonics from rotation should decrease with increasing order. It may be an indication of mechanical unbalance if the amplitude of the mechanical harmonics does not decrease with higher order, although this is not necessarily the case [17].

Vibrations of greater amplitudes tend to be found also at multiples of the rotational frequency that are related to certain machine parameters. For instance, if the turbine has four blades it is common to find a 4X component with high amplitude [18]. Other machine parameters that may appear in the vibration spectrums include:

- Number of generator stator slots per pole and phase
- Number of exciter rotor slots per pole and phase
- Number of guide vanes
- Number of generator poles
- Number of exciter poles

Equations 7.1 to 7.7 show at which frequencies the abovementioned parameters can contribute to peaks in the vibration spectrums.

$$f_{vib} = \begin{cases} f_e - f_{rot} \\ 6q_s \cdot f_e \\ f_{rot} \cdot p_n \\ (p_n \pm k) \cdot f_{rot}\,,\ (p_n \pm 2k) \cdot f_{rot} \\ t_b \cdot f_{rot} \\ g_v \cdot f_{rot} \\ n \cdot t_b \pm m \cdot g_v \end{cases} \quad [\text{Hz}] \quad \text{(Eq.7.1 – 7.7)}$$

Here q_s is the number of exciter rotor or generator stator slots per pole and phase, t_b is the number of turbine blades, g_v is the number of guide vanes and k, n and m are positive integers.

Eq.7.2 as well as Eq.7.3 can be applied using either the slots per pole and phase and electrical frequency of the exciter or generator. Eq.7.4 generates frequencies related to the number of exciter or generator poles with the addition or subtraction of an integer k or $2k$. This is related to the fact that the rotating shaft is not perfectly centered in the machines but subjected to small unbalances [17]. Hence the rotation is not strictly round and may contain traces of ovality, triangularity and so on. Peaks in the vibration spectrums due to unbalances in rotation are more likely to be found at frequencies obtained from a low value of k.

As stated in Eq.7.5 and Eq.7.6, the number of turbine blades and guide vanes can cause peaks in the vibration spectra as multiples of the rotational frequency. Linear combinations of these machine parameters can also lead to peaks in the vibration spectra in accordance with Eq.7.7.

2.3.3 Endurance

The ability of the FRBE stator to coupe with vibrations depends on vibration severity and exciter design. If vibration frequencies coincide with mechanical eigenfrequencies of the exciter stator, it can result in serious oscillations, putting the exciter stator at risk of damage [5].

The mechanical design plays a central role here as it determines the eigenfrequencies of the exciter stator, contributes to certain frequency content in the vibration spectra and affects the ability of the exciter stator to withstand vibrations. For example, it is crucial that the number of exciter poles does not result in an exciter electrical frequency for which any of the electrical harmonics from rectification coincide with a tangential eigenfrequency of the exciter stator. It is also vital that the attachment of the exciter stator is sufficient.

2.3.4 Requirements

As the FRBE is an outer-pole generator, vibration standards for generators are applied when assessing FRBE vibration levels. There are no separate vibration requirements developed particularly for exciters. An overview of the existing requirements on generator vibrations is provided below.

Norwegian Statkraft and Swedish Vattenfall have presented the *Nordic Generator Technical Requirements* (NGTR), in which some requirements regarding vibrations of the generator stator core are mentioned. The NGTR is subject to regular updates and the current version is from 2018. It states that the RMS amplitude of the vibrations of the generator stator core are not to exceed 2.0 mm/s in any direction for any frequency.

These requirements apply during any operation within the normal operation region [19]. The NGTR does not state any requirements on vibrations during transient operation. Also, it is noteworthy that the NGTR was not developed for evaluating exciters.

In addition to the NGTR, the International Organization for Standardization (ISO) have provided guidelines on acceptable vibration levels for different machine categories. The FRBE is classified as a group 4 machine, vertical machine sets with top bearing housings supported by the generator stator, in *ISO 20816-5: 2018*. The abovementioned ISO-standard contains two group specific criteria for evaluation of machine vibrations. The first criteria is regarding the vibration severity. In now outdated editions of the standard, machines were divided into evaluation zones A-D depending on how they performed on this note [20]. This division is explained in Table 1.

Table 1. Evaluation zones describing the severity of machine vibrations.

Evaluation zone	Explanation
Zone A	Acceptable, common for newly commissioned machines
Zone B	Acceptable for unrestricted long-time operation
Zone C	Unsatisfactory for long-term continuous operation
Zone D	Vibrations of sufficient severity to damage machine

In the current standard, ISO 20816-5: 2018, the evaluation zones have to some extent been replaced by action limits, describing when actions should be taken to limit machine vibrations. The first action limit is the limit of zone A/B-C, meaning when the machine no longer satisfies the requirements for long-term operation. When reaching the second action limit, zone C/D, the vibrations are so severe that they may damage the machine [20].

ISO 20816-5: 2018 also contains further categorization of the machine groups into sub-groups depending on the machine type. This division is done depending on the type of turbine utilized to drive the rotating shaft on which the generator is mounted [20]. Table 2 shows the action limits for a generator driven by a Kaplan turbine.

Table 2. ISO vibration action limits for a group 4 generator driven by a Kaplan turbine.

Action limit	Relative shaft vibration peak-to-peak [µm]			Bearing housing vibration v_{rms} [mm/s]		
	Turbine bearing	Gen. drive end bearing	Gen. non drive end bearing	Turbine bearing	Gen. drive end bearing	Gen. non drive end bearing
Zone A/B-C	110	170	170	1.1	0.6	1.0
Zone C/D	170	270	260	1.8	1.0	1.6

As seen in Table 2 the vibration requirements for group 4 machines include three vibration measurements. These are located at three different bearings, one near the turbine and two on each end of the generator (see Figure 9). Out of these it is only the generator non drive end bearing that is located near the exciter [20].

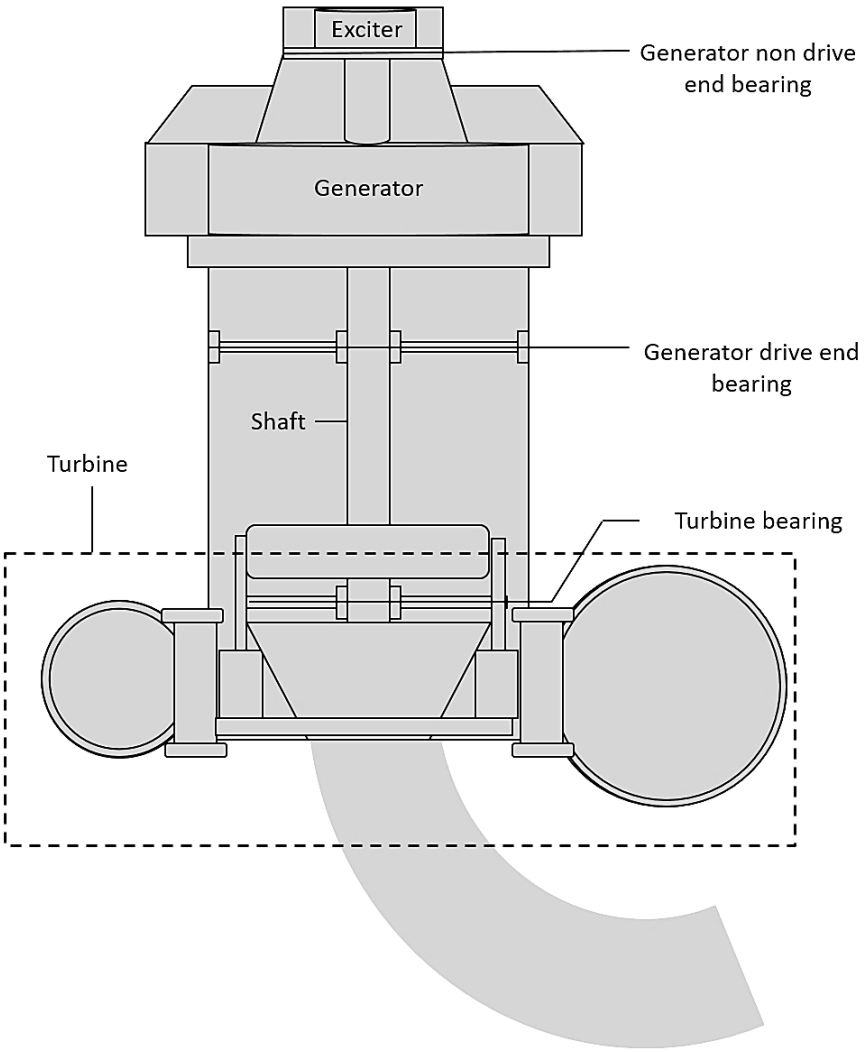

Figure 9. Illustration of where the bearing housings are located.

Regarding the second criteria of ISO 20816-5: 2018 it concerns the change in vibration levels and vibration trends over time. Change in vibration levels can come in many shapes and may indicate an existing or oncoming fault [20]. In order to make adequate evaluations of this second criteria the machine must however be monitored over a longer period of continuous operation. No such opportunities have been available within the scope of this thesis, why this criteria has not been checked.

2.3.5 Previous work

Since vibrations on the exciter stator have a negative impact on the excitation system reliability it is desirable to mitigate them. Attempts to achieve this, by mitigating the pulsations in the exciter air gap torque, have been the focus of many of the previous works about FRBE systems. It has been shown that torque pulsations can be mitigated in various ways.

For instance, a six-phase excitation system, utilizing twelve-pulse active rectification, result in less severe torque pulsations than a three-phase, six-pulse system. Measurements done on a test rig at Uppsala University have shown that the shift from six-pulse to twelve-pulse rectification could lead to more than 70% reduction in vibration severity [11]. One addition advantage is that the two thyristor bridges of a six-phase, twelve-pulse excitation system can be connected in different configurations, which can contribute to further reduction [14]. The major drawback with these six-phase, twelve-pulse solutions is that the industry standard is three-phase and six-pulse.

Another design characteristic which seems to affect the torque pulsations is the exciter number of rotor slots per pole and phase. Simulations of the behavior of a FRBE have shown that a higher number of slots per pole and phase reduces the torque pulsations notably, both for three-phase and six-phase systems. However, as some issues were identified in the underlying model, it is not clear just how extensive the reduction would be [12]. One additional solution that has been suggested is to apply a larger air gap in combination with a slight shift of the exciter stator poles to counteract the torque pulsations [6].

In addition to the abovementioned design parameters, it has been shown that operation at lower firing angles yields a positive result in terms of mitigating the air gap torque pulsations [11]. Limiting operation to lower firing angles does however result in a reduction of the available ceiling voltage, which in turn makes the system slower in response [10]. Such a solution would therefore be compromising on exciter performance.

3. Method

In this chapter the method used for measuring, analyzing and evaluating vibrations on the stator of a FRBE is presented. It consists of three parts. The first part describes how vibration measurements were carried out on an actual FRBE stator. It includes listing and installation of equipment and descriptions of the applied settings and studied load conditions. The second part focuses on analysis of the frequency content and origins of the recorded vibrations. Meanwhile, the third part describes how the observed vibrations were evaluated.

3.1 On-site measurement

To enable analysis of the frequency content of the stator vibrations of a FRBE, vibration recordings were conducted at a hydropower plant. Below follows a description of how these recordings were carried out.

3.1.1 Equipment and installation

The following equipment was used to measure vibrations on the exciter stator:

- Eight accelerometers with magnetic feet for attachment
- Two metal blocks
- Industrial glue
- Accelerometer transducer box
- Measurement case containing a computer equipped with DiaGen software for vibration recordings and analysis
- Eight cables for connecting the accelerometers to the accelerometer transducer box
- Nine coaxial cables for connecting the accelerometer transducer box to the channels and voltage supply of the measurement case

Accelerometers were attached to the exciter stator, intending to measure the absolute vibration velocity [mm/s]. When the mobile mass of the accelerometer moves in relation to its inertial reference mass, an electrical charge arises that is proportional to the movement. This electrical charge can then be converted into measurements of the absolute acceleration [mm/s^2]. Measurements of the absolute vibration velocity can then be obtained by integrating the signal from the accelerometer [17].

The accelerometers were placed around two points, located 90 degrees apart. It is common practice to select the first point in the upstream direction, denoted Y, whereas the second point, X, is shifted 90 degrees clockwise from Y [17]. However, the upstream direction at site provided little floor space for equipment, whereby -Y and -X were used instead. This labeling is illustrated in Figure 10.

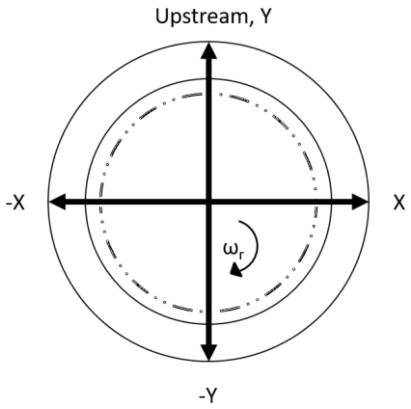

Figure 10. Location of measuring points on a rotating exciter, as seen from above.

The accelerometers were attached to the exciter stator frame using their magnetic feet. Firm connection between the accelerometers and the stator frame was ensured to avoid faulty measurements due to poor attachment. The accelerometers measuring radial vibrations could be attached directly to the stator frame. However, to be able to measure tangential vibrations, metal blocks had to be glued onto the stator frame to which the accelerometers could be attached. This was done using industrial glue.

A total of seven accelerometers were placed on the exciter stator frame near the -Y and -X axis in order to get an overview of the vibrations the stator was subjected to. One additional accelerometer was mounted on the exciter enclosure. Figure 11 illustrates where the accelerometers were placed in relation to the nearest axis.

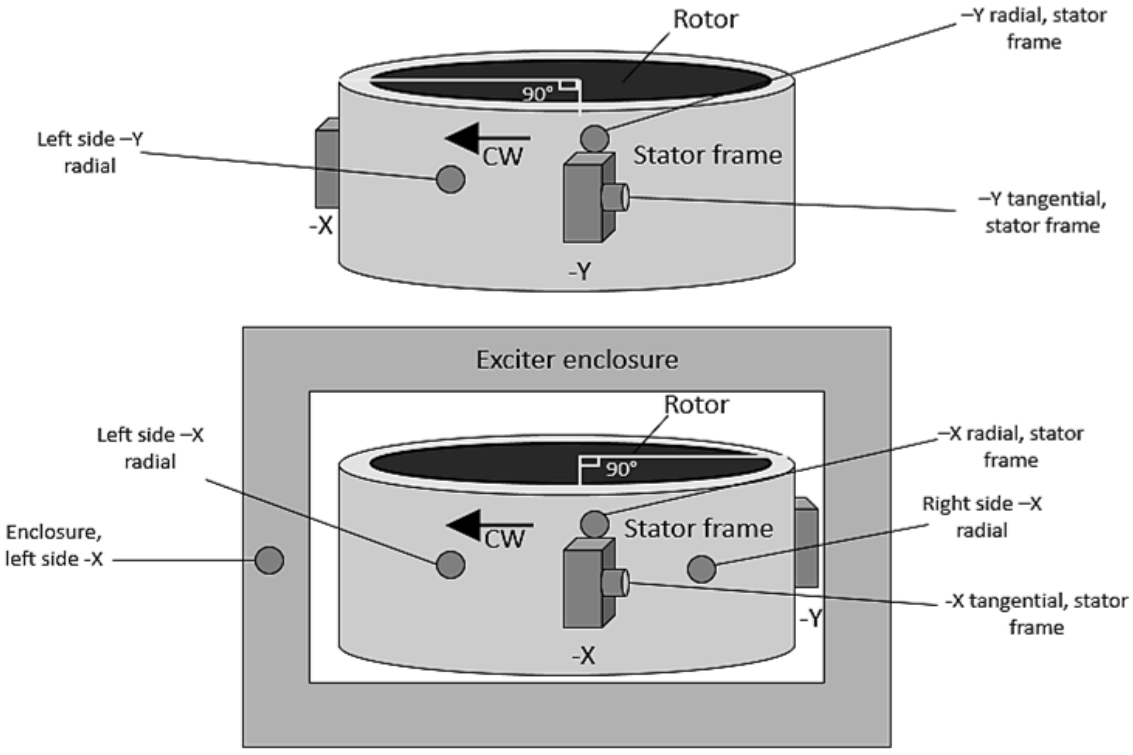

Figure 11 a) Placing of accelerometers when measuring vibrations on the exciter stator near the -Y axis. b) Near the -X axis. CW indicates clockwise rotation.

After having attached the accelerometers to the exciter stator frame and exciter enclosure, each accelerometer was connected, via the designated cable, to an input channel in the accelerometer transducer box, where the accelerometer signals were converted from measurements of acceleration to velocity measurements. Using coaxial cables, the output channels of the accelerometer transducer box were then connected to the corresponding input channels of the measurement case. Finally, one additional coaxial cable was used to connect the accelerometer Transducer box to the measurement case 24V DC voltage supply. The installation of the equipment can be found in Figure 12.

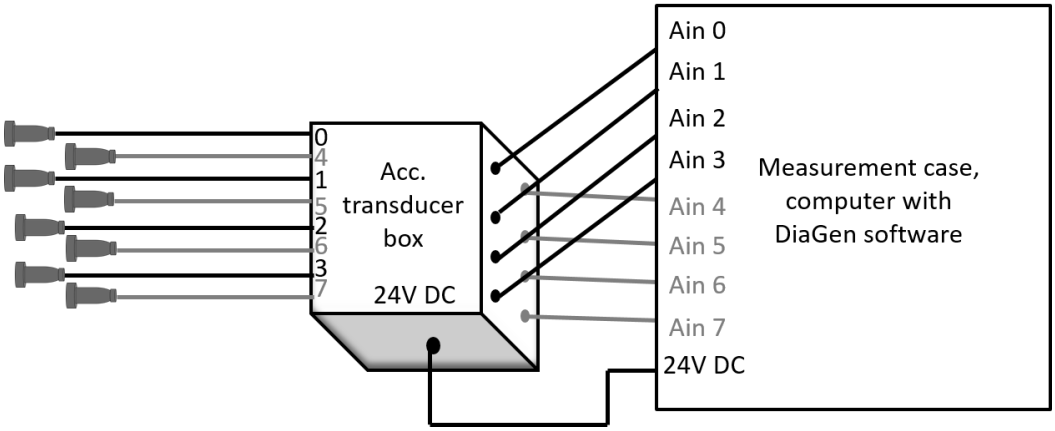

Figure 12. Installation of equipment.

3.1.2 Vibration recordings

After having rigged the equipment, vibrations were recorded during different load conditions in the vibration analysis software DiaGen. The recordings were started manually and contained 60 seconds worth of vibration data. Each recording was done at a sampling rate of 2500 Hz, which resulted in a total of 150 000 measurements per recording and accelerometer. Vibrations on the exciter stator were recorded and analyzed during the following conditions:

- Exciter running at nominal speed but without excitation
- Exciter running in no load, thyristor mode, with fixed exciter field current set points
- Exciter running in 60 % load, thyristor mode, with a dynamic exciter field current set point
- Exciter running in full load, thyristor mode, with dynamic exciter field current set points
- Exciter running in full load, diode mode

The vibration recording of the exciter running at nominal speed without excitation was done in order to get data on the purely mechanical vibrations with no electrical interference. In no load and full load, thyristor mode, vibration recordings were

conducted with varying fixed or dynamic exciter field current set points in order to see the impact of the firing angle on vibration severity.

Vibration recordings in no load were carried out with the fixed exciter field current set points 1.8, 1.9, 2.0, 2.1, 2.2 and 2.3. In full load, thyristor mode, the applied dynamic exciter field current set points were 1.3, 1.4 and 1.6. As for the vibration recording in 60% load, thyristor mode, the purpose was to provide a lower load measurement. In this case, a dynamic exciter field current set point of 1.4 was used. For recollection, the difference between fixed and dynamic exciter field current set point is explained in Chapter 2, Part 2.2.3.

For comparison, a recording was also carried out in full load, diode mode. During this run, the thyristors were fired at a 10 degree firing angle, which was the minimum firing angle for the firing card. From previous measurements, carried out at another thyristor-fed unit, it has been concluded that the vibration levels observed with thyristors operating at minimum firing angle have the same magnitude as the vibrations of an identical diode-fed unit [21]. To enable estimation of firing angles for the tests in thyristor mode, readings of the RMS AC exciter voltage and of the generator field voltage were taken. The voltage values, together with active and reactive power levels for each load case, were obtained from on-site sensors and excitation system measures.

It is worth mentioning that when vibration recordings were carried out in full load, thyristor mode, the exciter had been running overnight in steady state with unchanged control settings. All other recordings were carried out just a few minutes after the desired settings were applied.

3.2 Frequency analysis

Out of the recorded 60 seconds, a data segment of 4 seconds, corresponding to about 10 shaft rotations, was selected for analysis. This was done in order to avoid unwanted smearing effects. Based on the selected data segment, vibration spectrums were generated in DiaGen for each run, using the built in Fast Fourier Transform (FFT) function. A graphical study of the spectrums was then carried out, where peak frequencies and their relation to the rotational frequency 1X was noted. The graphical information was used, together with known machine parameters and the equations presented in Chapter 2, in an attempt to determine the vibration origins. When studying the vibration spectrums in DiaGen, a frequency range of 0.5-1000 Hz and a resolution of 4000 lines was used, being the highest available resolution for the chosen data segment. The highest frequency that could be accurately represented, given the sampling rate of 2500 Hz, was 1000 Hz.

As the vibration spectrums generated in DiaGen represented the vibration amplitudes as peak values, the FFT data was extracted and the amplitudes were converted to RMS values in Matlab.

3.3 Evaluation

The observed vibration frequencies and amplitudes were evaluated from two perspectives. Part of the evaluation consisted of comparing the observed vibrations to the NGTR and ISO requirements. Fulfillment of the NGTR was evaluated by calculating the RMS amplitude of the unfiltered vibration signals in all directions for all cases. The RMS vibration amplitudes of the FFT-filtered vibration signals were also evaluated on this point. This was done in order to see if the limit of 2.0 mm/s, RMS, was ever exceeded. To enable evaluation of the ISO requirements (see Table 2), additional data on vibration levels on bearing housings was provided by the hydropower plant owner. Unfortunately, due to a mismatch in resolution, data on bearing housing vibrations was only available for the runs in full load, thyristor mode. Since the evaluation of the ISO requirements was executed from an exciter perspective, focus was limited to the generator non drive end bearing and the generator drive end bearing.

Mechanical analysis, performed by experts at Voith Hydro AB, were also used when evaluating the observed vibrations. From the mechanical analysis, estimates of the exciter stator tangential eigenfrequencies were provided. Unfortunately, no estimates of the radial eigenfrequencies were available. To conclude whether or not the measured vibrations put the exciter stator at risk of damage, the tangential eigenfrequencies were put in relation to the observed peak frequencies and vibration amplitudes obtained from the on-site recordings.

4. Data

This part presents the data used when identifying vibration origins, calculating firing angles and evaluating the observed vibrations. Load conditions are specified for the 60% load and full load cases. The chapter also contains a summary of the relevant data on bearing housing vibrations that was provided by the hydropower plant owner. Last but not least, the exciter stator tangential eigenfrequencies are displayed.

Table 3 presents machine parameters of the studied FRBE and the related hydroelectric generator and Kaplan turbine. By insertion into the equations presented earlier in Chapter 2, these parameters were used for identifying probable vibration sources.

Table 3. Machine parameters of the studied FRBE and the related hydroelectric generator and Kaplan turbine.

Machine parameter	Quantity	Variable
Number of turbine blades	5	t_b
Number of guide vanes	24	g_v
Rotational speed of shaft	166.67 rpm	n_s
Rated power of generator	52 MVA	S_r
Generator electrical frequency	50 Hz	f_{eg}
Number of generator poles	36	p_{ng}
Number of generator stator slots	243	Q_{sg}
Number of generator slots per pole and phase	2.25	q_{sg}
Exciter electrical frequency	25 Hz	f_{ee}
Number of exciter poles	18	p_{ne}
Number of exciter rotor slots	162	Q_{se}
Number of exciter slots per pole and phase	3	q_{se}
Number of exciter stator attachment points	16	-
No load exciter field current base value	9.0 A	$I_{fe,NL}$

Table 4 clarifies the studied load conditions. The measurements of active and reactive power were obtained from an on-site interface.

Table 4. Specification of the studied load conditions.

Load condition	Active power	Reactive power
No load	-	-
60 % load	28.0 MW	13.8 MVAr
Full load, thyristor mode	42.3 MW	20.5 MVAr
Full load, diode mode	46.5 MW	20.0 MVAr

For the runs in no load, readings of the RMS AC exciter field voltage, $U_{fe,AC}$, and the generator field voltage, U_f, were acquired from sensor signals registered in a computer interface. An on-site interface provided similar readings for the runs in 60% load and full load thyristor mode. These voltages were later on used to estimate the firing angles with the different settings. The readings are presented in Table 5. It ought to be noted that, although in theory they should be the same, the generator field voltage readings varied slightly also at unchanged load. This deviance may be attributed to temperature related variations in field winding resistance or to the usage of instantaneous readings instead of average values.

Readings of the generator field current, I_f, for each load case and setting were also provided by the abovementioned on-site interface. In addition to this, the exciter field currents, $I_{fe,DC}$, were obtained from sensor signals registered in the same computer interface as the no load voltages. The generator field currents and DC exciter field currents are shown in Table 5 as well.

Table 5. Readings of field currents and field voltages.

Load case	$U_{fe,AC}$	U_f	$I_{fe,DC}$	I_f
No load 1.8 (FF_sp)	137 V	78 V	16.4 A	496 A
No load 1.9 (FF_sp)	148 V	72 V	17.3 A	496 A
No load 2.0 (FF_sp)	157 V	68 V	18.1 A	496 A
No load 2.1 (FF_sp)	170 V	65 V	19.0 A	496 A
No load 2.2 (FF_sp)	182 V	61 V	19.8 A	496 A
No load 2.3 (FF_sp)	193 V	60 V	20.7 A	496 A
60% load 1.4 (FD_sp)	130 V	106 V	20.5 A	875 A
Full load 1.3 (FD_sp)	149 V	146 V	23.4 A	1073 A
Full load 1.4 (FD_sp)	168 V	152 V	25.1 A	1075 A
Full load 1.6 (FD_sp)	209 V	153 V	28.8 A	1068 A

For the purpose of putting the severity of vibrations in relation to ISO 20816-5: 2018, the hydropower plant owner provided untreated data on bearing housing vibrations that were recorded during the same days as the vibration measurements were conducted on the exciter stator. This data contained roughly one measurement every 15th minute. Since the recorded vibration of the exciter stator only covered 60 seconds worth of measurements, the resolution did not match. Hence, data on bearing housing vibrations could only be used for the full load, thyristor mode cases. Although only 4 seconds worth of vibration measurements were analyzed for each setting, the exciter had been running with the same settings and at constant load overnight. It was thus assumed that the analyzed 4 seconds were representative for a longer period of time.

The provided data on bearing housing vibrations consisted of peak to peak measurements of the relative shaft vibration in the radial positive Y and X direction (see Figure 9 and Figure 10). Due to small variations in the provided data, a mean or median value was considered to be more reliable than a point value. The maximum value was also of interest in order to determine whether the ISO requirements on vibrations were fulfilled at all registered times. Hence, for all runs in full load thyristor mode, the mean, median and max peak to peak relative shaft vibrations were calculated using the untreated bearing housing vibration data registered overnight. The resulting data on bearing housing vibrations is shown in Table 6 and Table 7.

Table 6. Relative peak to peak shaft vibrations of the generator non drive end bearing with the exciter running at full load in thyristor mode.

	Y radial, relative S_{p-p}[µm]			X radial, relative S_{p-p}[µm]		
	Mean	Median	Max	Mean	Median	Max
Full load 1.3 (FD_sp)	137.2	139	140	156.8	160	162
Full load 1.4 (FD_sp)	140.3	142	150	161.2	164	167
Full load 1.6 (FD_sp)	140.1	142	145	161.2	164	167

Table 7. Relative peak to peak shaft vibrations of the generator drive end bearing with the exciter running at full load in thyristor mode.

	Y radial, relative S_{p-p}[µm]			X radial, relative S_{p-p}[µm]		
	Mean	Median	Max	Mean	Median	Max
Full load 1.3 (FD_sp)	63.8	67	70	48.2	51	52
Full load 1.4 (FD_sp)	64.4	67	88	49.4	51	86
Full load 1.6 (FD_sp)	63.9	67	69	48.7	51	53

Last of all, the exciter stator tangential eigenfrequencies, obtained from the mechanical analysis are listed in Table 8.

Table 8. Tangential eigenfrequencies of the studied exciter stator frame and machine top.

Frequency	Region
33.7 Hz	Stator frame
47.6 Hz	Stator frame and machine top
92.4 Hz	Stator frame
141.7 Hz	Stator frame and machine top
172.0 Hz	Stator frame
209.8 Hz	Stator frame and machine top
268.7 Hz	Stator frame
377.3 Hz	Stator frame

The eigenfrequencies displayed in Table 8 are all significant tangential eigenfrequencies in the range 0-450 Hz of the exciter stator frame, with and without attachment, enclosure etcetera.

5. Results and analysis

In this chapter the results from the on-site measuring and frequency analysis are presented. This includes mapping of the observed frequency content, identification of potential vibration origins and evaluation of firing angles and field current levels in relation to vibration severity. For the latter, a sensitivity analysis focusing on data segmentation and placing of accelerometers is presented. Last but not least, the observed vibrations are evaluated in relation to the NGTR and ISO requirements and to the exciter stator tangential eigenfrequencies.

5.1 Frequency content and vibration origins

The vibration spectrums yielded from the FFT function in DiaGen, based on 10 shaft rotations, are presented in Figure 13 to Figure 20. For simplification, only the radial and tangential vibrations are included. To avoid confusion it is worth noting that the scales have been adapted to fit the frequency and amplitude range for each recording. It is recommended that extra attention is devoted, mainly to the scale of the Y axis.

5.1.1 Nominal speed without excitation

Figure 13 shows the vibration spectra obtained when the exciter was running at nominal speed without excitation.

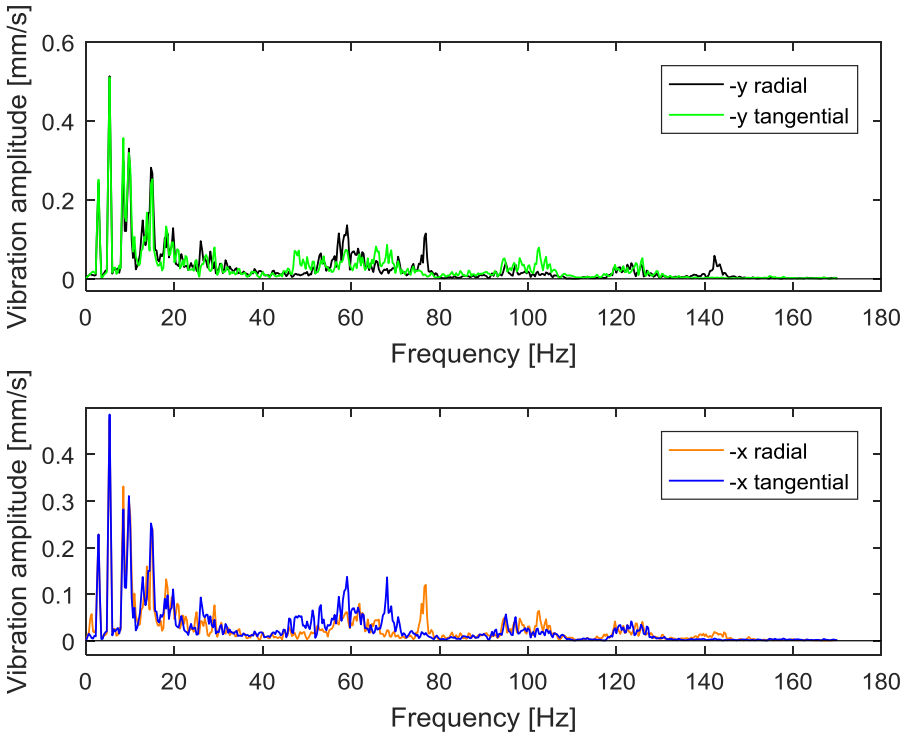

Figure 13. Spectra of vibrations recorded when the exciter was running at nominal speed without excitation.

The peaks seen in the spectra represent the purely mechanical part and the highest peaks are found at the frequencies 2.812 Hz, 5.312 Hz, about 9.7 Hz and 15.0 Hz. Peaks also occur at frequencies around 50 Hz and just below 60 Hz, 70 Hz and 80 Hz, albeit of lower amplitude. Insertion of the rotational speed of the shaft, presented in Table 3, into Eq.5 yields:

$$f_{rot} = \frac{n_s}{60} \rightarrow \frac{166.67}{60} \approx 2.778\ Hz$$

Thus the 2.812 Hz component seen in Figure 13 is the rotational frequency 1X. The higher 5.312 Hz component corresponds to 2X. Why this component is larger than the 1X component has not been further investigated. The same goes for the origins of observed non-integer multiples of 1X. This since the main purpose of the vibration recordings in nominal speed and no excitation was to act as a purely mechanical reference to assist other evaluation.

5.1.2 No load in thyristor mode

In Figure 14 the vibration spectra yielded in no load with the fixed exciter field current set point 1.8 is displayed. To represent the range of exciter field current set points applied Figure 15 shows the vibration spectra with the fixed exciter field current set point 2.3.

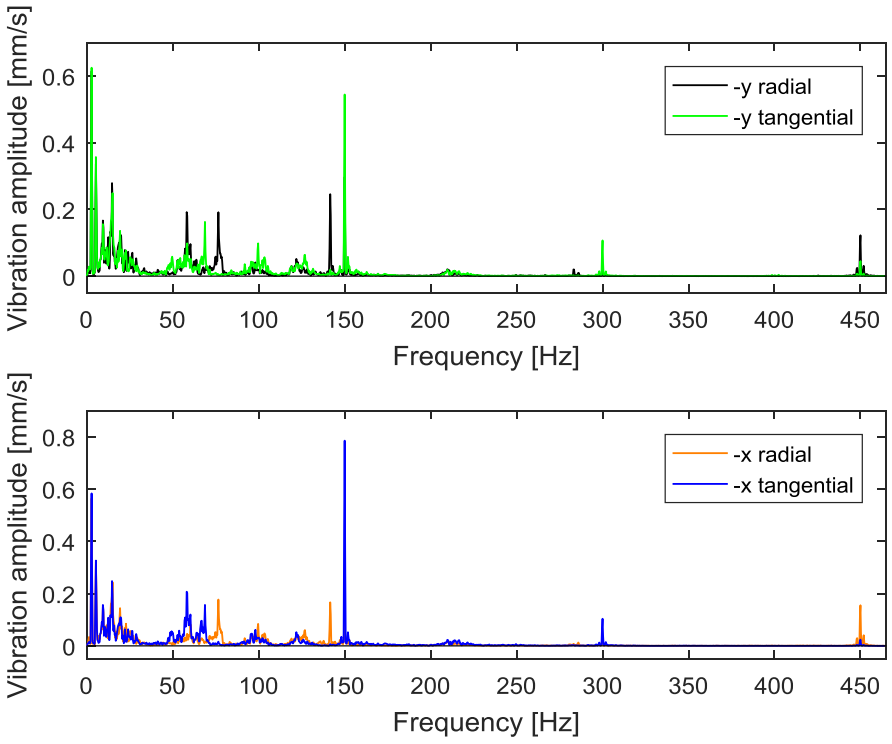

Figure 14. Spectra of vibrations recorded with the exciter running in no load, thyristor mode. Exciter field current set point is 1.8, fixed.

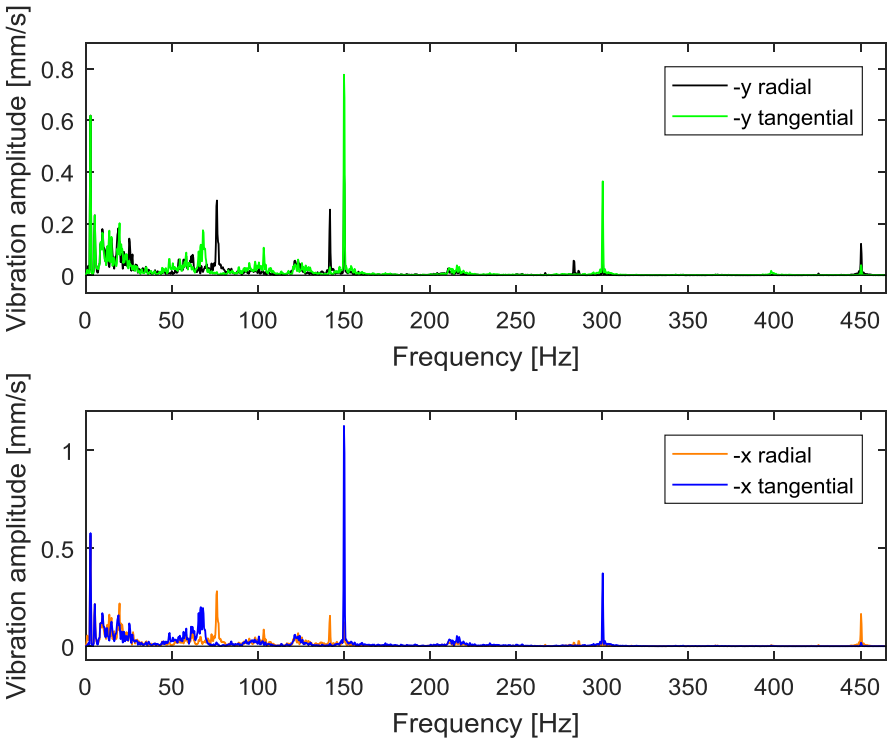

Figure 15. Spectra of vibrations recorded with the exciter running in no load, thyristor mode. Exciter field current set point is 2.3, fixed.

When comparing Figure 14 to Figure 15 it is seen that the spectrums contain peaks at the same frequencies. However the amplitudes of said peaks increase when the fixed exciter field current set point is assigned a higher value. Most of this increase occurs in the tangential -Y and -X directions at frequencies 150 Hz and 300 Hz. When inserting the electrical frequency of the exciter, found in Table 3, into Eq.4 it becomes clear that the peaks at frequencies 150 Hz and 300 Hz originate from the rectification pulses.

$$f_n = 6n \cdot f_e \rightarrow 6n \cdot 25 = 150n\ Hz$$

This makes 150 Hz and 300 Hz the first and second order electrical harmonic frequency. Also at the third order electrical harmonic frequency, 450 Hz, a peak is present both in Figure 14 and Figure 15. As stated in the theory, presented in Chapter 2, the amplitude of these harmonics decreases with increasing order.

Considering the fact that the 450 Hz peak is very visible also in the radial directions, it is likely to have more than one source. Insertion of the number of exciter slots per pole and phase and the exciter electrical frequency, both presented in Table 3, into Eq.7.2 gives:

$$6q_s \cdot f_e \rightarrow 6 \cdot 3 \cdot 25 = 450\ Hz$$

Thus, the slots on the exciter rotor may also contribute to this peak.

Peaks that appear from just below 50 Hz up to about 65 Hz may originate from small deviations in exciter rotor roundness. These frequencies are namely found in the more plausible range covered by Eq.7.4, after inserting the number of exciter poles and the rotational frequency (see Table 3).

A 100 Hz peak is also visible in Figure 14 and Figure 15. The peak at 100 Hz also has multiple sources. As it is double the grid electrical frequency of 50 Hz it is an expected peak. In addition to this it may be a consequence of the main generator poles. When multiplying the number of generator poles with the observed rotational frequency (see Table 3), as stated in Eq.7.3, a frequency of 100 Hz is obtained:

$$f_{rot} \cdot p_{ng} \rightarrow 2.778 \cdot 36 \approx 100.0\ Hz$$

In addition to this, small peaks are found in the range between 20 Hz and 25 Hz. They appear to be integer multiples of 1X since the frequency distance between peaks is approximately 1X. One of these peaks is thought to be the subtraction of the rotational frequency from the exciter electrical frequency (see Table 3). Insertion of said data into Eq.7.1 yields:

$$f_e - f_{rot} \rightarrow 25 - 2.778 \approx 22.22\ Hz$$

Peaks are found also at 69.4 Hz in the tangential directions and 141.7 Hz in the radial directions. No clear source of the 69.4 Hz peak could be identified. From Table 8, presented earlier in Chapter 4, it can be seen that 141.7 Hz is one of the tangential exciter stator eigenfrequencies obtained from mechanical analysis. However it mainly occurs in the radial directions and is barely present in the tangential measurements.

In addition to the abovementioned peaks, the vibration recordings in no load contain many of the peaks observed in nominal speed and no excitation. However, despite a relatively high peak at the rotational frequency, the increasingly large 150 Hz component dominates all vibration spectrums in no load, at least in the tangential –X direction. When the exciter field current set point is set to 2.0, the 150 Hz component becomes greater than that of the rotational frequency also in the tangential –Y direction.

5.1.3 60 % load in thyristor mode

The vibration spectra obtained at 60 % load is seen in Figure 16. The dynamic exciter field current set point is 1.4. Specifications of the load in terms of active and reactive power can be found in Table 4 presented earlier in Chapter 4.

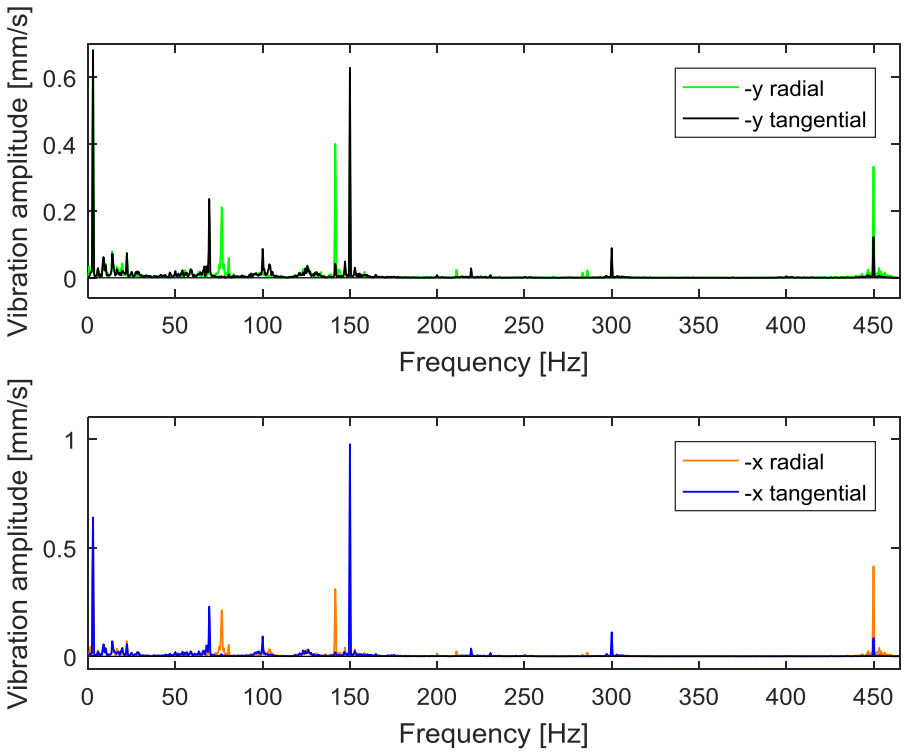

Figure 16. Spectra of vibrations recorded with the exciter running in 60 % load, thyristor mode. Exciter field current set point is 1.4, dynamic.

As is seen when comparing Figure 16 to Figure 14 and Figure 15, the frequencies of the peaks present in the spectra have not changed as the load was increased. Their amplitudes however, both in terms of absolute values and relations in between peaks, look somewhat different than in no load. For instance, the 450 Hz component has increased to a level higher than that of the 300 Hz component, supporting the hypothesis that the peak has multiple sources. The peaks at 69.4 Hz and 141.7 Hz have also increased whereas the 150 Hz component from rectification is almost unchanged and has even decreased compared to the peak in Figure 15. In the tangential –X direction, the 150 Hz peak still has the greatest amplitude in the vibration spectra. However, the same peak has decreased in the tangential –Y direction to a level below that of the peak at the rotational frequency.

5.1.4 Full load in thyristor mode

Figure 17, Figure 18 and Figure 19 show the vibration spectrums yielded in full load thyristor mode with a dynamic exciter field current set point of 1.3, 1.4 and 1.6 respectively. It is worth observing the changing scale of the Y axis describing the vibration amplitude.

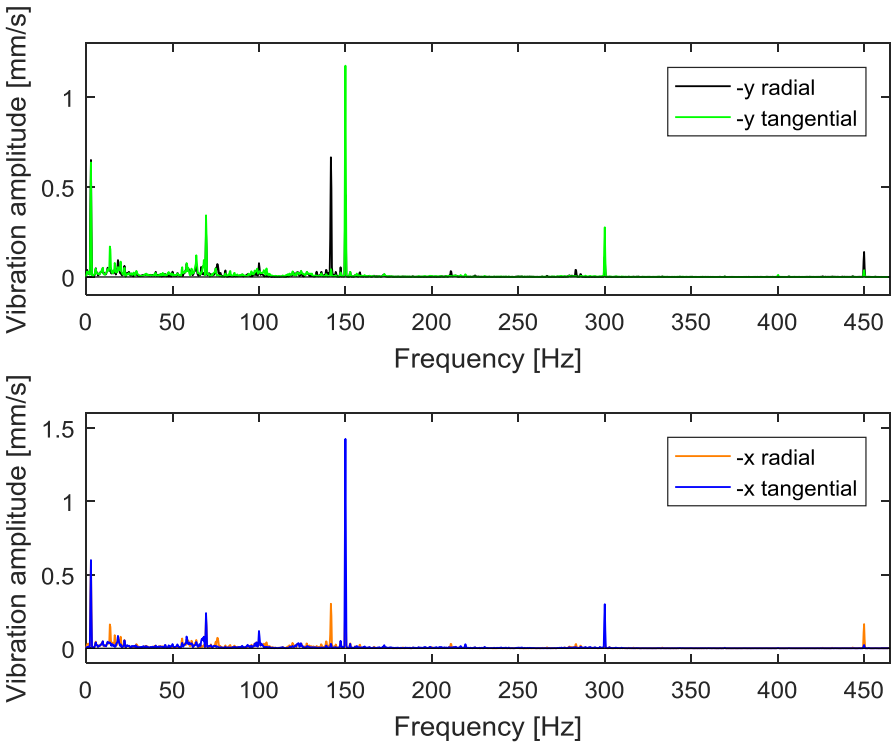

Figure 17. Spectra of vibrations recorded with the exciter running in full load, thyristor mode. Exciter field current set point is 1.3, dynamic.

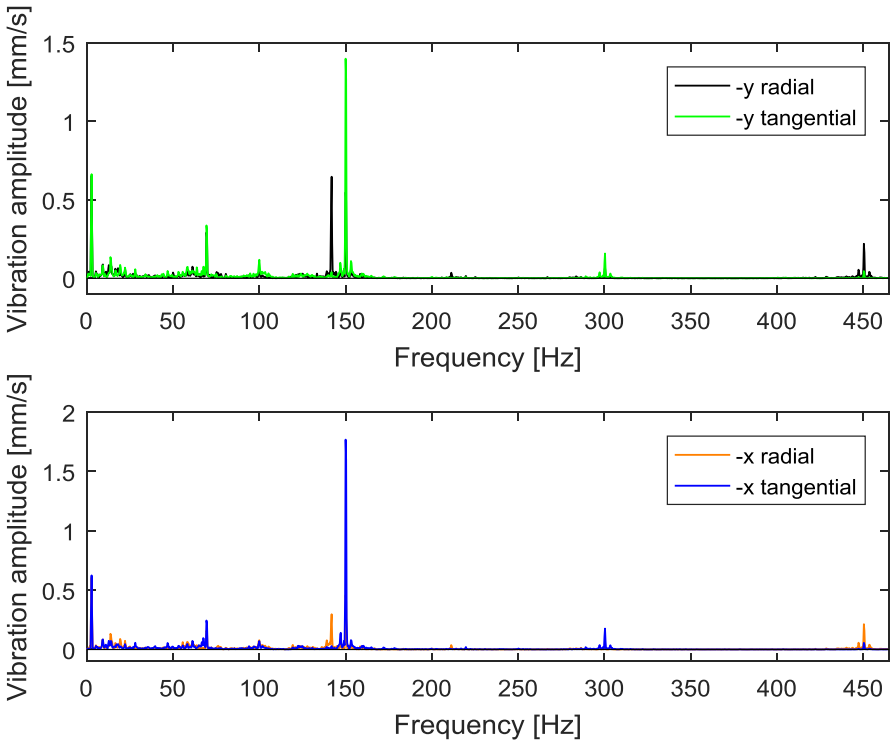

Figure 18. Spectra of vibrations recorded with the exciter running in full load, thyristor mode. Exciter field current set point is 1.4, dynamic.

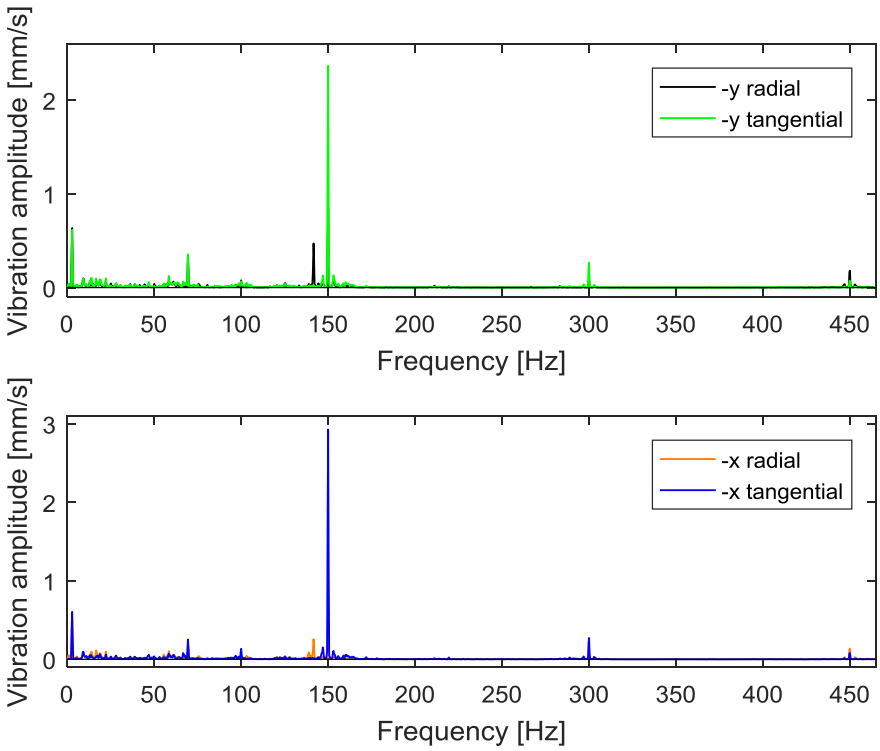

Figure 19. Spectra of vibrations recorded with the exciter running in full load, thyristor mode. Exciter field current set point is 1.6, dynamic.

The vibration spectrums presented in Figure 17, Figure 18 and Figure 19 contain peaks at the same frequencies as in the 60 % load case. In addition to this, a peak around 14 Hz is visible in the radial -Y direction, mainly in Figure 17 and Figure 18. This peak is likely to originate from the turning of the turbine blades as insertion of the number of turbine blades, found in Table 3, into Eq.7.5 gives:

$$t_b \cdot f_{rot} \rightarrow 5 \cdot 2.778 = 13.89\ Hz$$

The main difference from the vibrations recorded in 60 % load is the fact that a significant increase in amplitude of the 150 Hz component has taken place. Moreover, the increased load has led to a higher amplitude also of the 300 Hz peak. From Table 5 it becomes clear that the generator field current has increased from 875 A to a level of about 1070 A, supposedly leading to more severe pulsations of the air gap torque.

When instead comparing the different cases in full load, thyristor mode, there are signs of an exponential pattern. Comparison between a dynamic exciter field current set point of 1.3 and 1.4 only shows a slight increase in the amplitude of the 150 Hz peak, whereas the same peak undergoes an increase in amplitude of almost 70% when the dynamic exciter field current set point is increased from 1.4 to 1.6.

5.1.5 Full load in diode mode

Figure 20 shows the vibration spectra obtained at full load in diode mode. It is once again worth noting the scale of the Y axis.

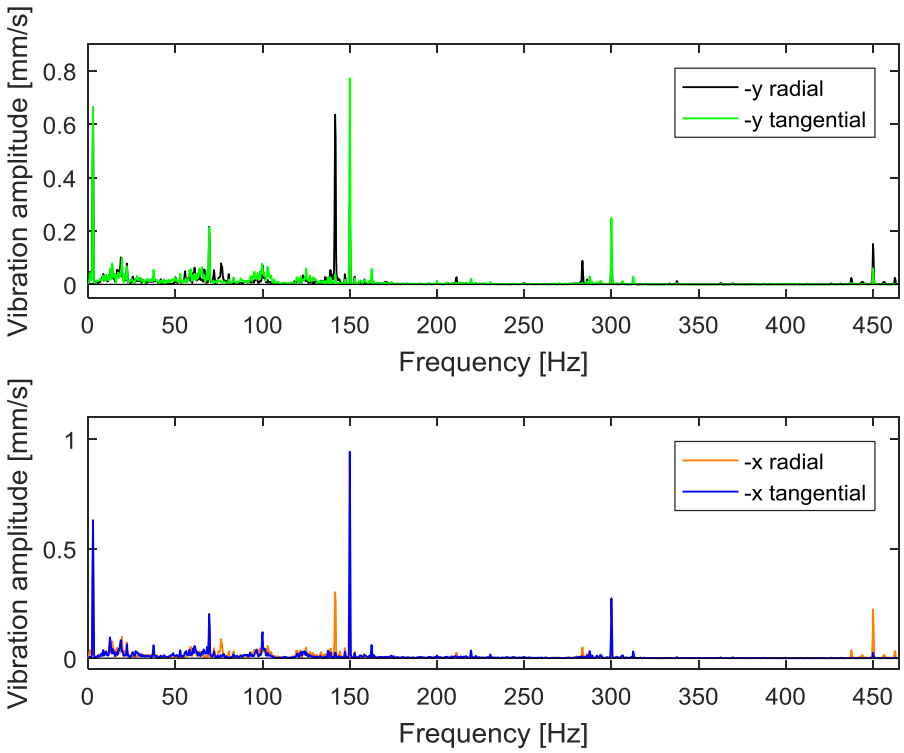

Figure 20. Spectra of vibrations recorded with the exciter running in full load, diode mode.

Peaks appear at the same frequencies in full load diode mode as in 60 % load and full load thyristor mode. Although the load is somewhat higher than in full load thyristor mode, the 150 Hz peak amplitude has been significantly reduced. It is however still the highest peak in the vibration spectra. The amplitude of the peak at 150 Hz in full load, diode mode, is in the same range as for the 60 % load case in thyristor mode.

With the increased load, an increase in the amplitude of the peaks at 69.4 Hz and 141.7 Hz has also been observed. Since the peak at 141.7 Hz is still high despite the fact that there has been a great reduction of the 150 Hz component, it appears that the increase in amplitude is not governed by the firing of the thyristors. The source of the peak at 69.4 Hz is still unknown, but the finding suggests that the amplitude of this peak, like that of the 141.7 Hz peak, depends mainly on the load conditions.

5.1.6 Summary of vibration origins

In Table 9, a summary of the observed peak frequencies and the corresponding vibration origins is presented. The relation between peak frequencies and the rotational frequency 1X is also displayed.

Table 9. Summary of observed peak frequencies and corresponding vibration origins.

Frequency	1X-multiple	Direction	Origin
2.78 Hz	1	Radial and tangential	Activities that occur once per shaft rotation
13.89 Hz	5	Radial	Turning of the turbine blades
47-65 Hz	17-23.4	Radial and tangential	Minor deviances in rotor roundness
64.9 Hz	23.3	Tangential	Unknown
100 Hz	36	Radial and tangential	Generator poles and double electrical frequency of the grid
141.7 Hz	51	Radial	Unknown, but is a *tangential* mechanical eigenfrequency of the exciter stator frame
150 Hz	54	Tangential	Torque pulsations from rectification
300 Hz	108	Tangential	Torque pulsations from rectification
450 Hz	162	Radial and tangential	Exciter rotor slots per pole and phase and torque pulsations from rectification

It is worth pointing out that the vibration sources mentioned in Table 9 is by no means an exhaustive list. There may exist additional vibration sources that could not be identified in this study.

5.2 Firing angle and vibration severity

The firing angles corresponding to each setting in no load, 60% load and full load thyristor mode were estimated by inserting data from Table 5 into Eq.1. In diode mode, the thyristors were fired with the minimum firing angle of 10 degrees. In Figure 21, the applied firing angles are presented for each case along with the amplitude of the 150 Hz vibrations in the –X tangential direction, where the most severe vibrations were observed. A similar behavior was observed also in the –Y tangential direction.

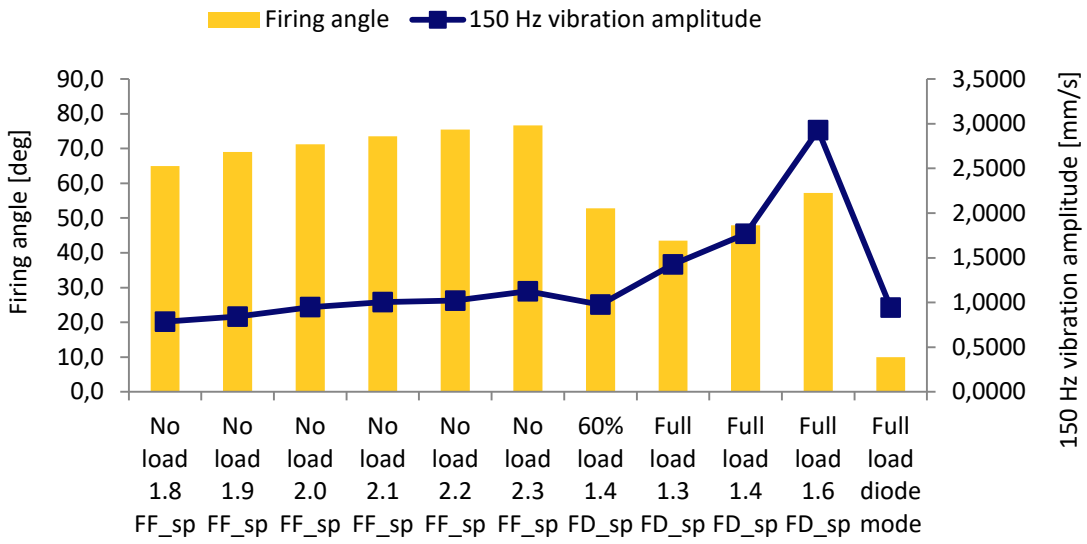

Figure 21. Estimated firing angles and observed amplitude of the –X tangential 150 Hz vibrations.

When comparing Figure 21 with the exciter field current levels and the generator field current levels in Table 5, it can be seen how the change in firing angle keeps the generator field current constant as the exciter field current is altered at unchanged load. From Figure 21 it becomes clear that higher firing angles were applied in no load than in 60% load and full load thyristor mode.

As brought in Chapter 2, higher firing angles are expected to result in higher peaks at 150 Hz due to more severe torque pulsations. In Figure 21 it can be seen that the severity of the 150 Hz vibrations increases with an increase in firing angle at constant load. In full load, thyristor mode, it appears that an increase in firing angle may even lead to an exponential increase in amplitude of the 150 Hz vibrations. This is similar to the expected behavior of the torque pulsations, mentioned in Chapter 2, Part 2.2.4.

Comparison between the firing angles and vibration amplitudes in Figure 21 provides further indications that vibration amplitudes depend not only on firing angle but also on load conditions. For instance, higher vibration levels are observed in full load, thyristor mode than in 60% load, thyristor mode. This is the case since the higher generator field current required in full load, thyristor mode, outweighs the higher firing angle applied in 60% load, thyristor mode. Also, in diode mode, with the highest studied load and the lowest firing angle, the amplitude of the 150 Hz vibrations is in the same range as in 60% load. From all this it can be concluded that the severity of the vibrations from rectification depends on the interplay between generator field current and firing angle.

For more visualization, Figure 22 and Figure 23 show the –X tangential 150 Hz vibration amplitude along with the exciter stator field current and the generator field current.

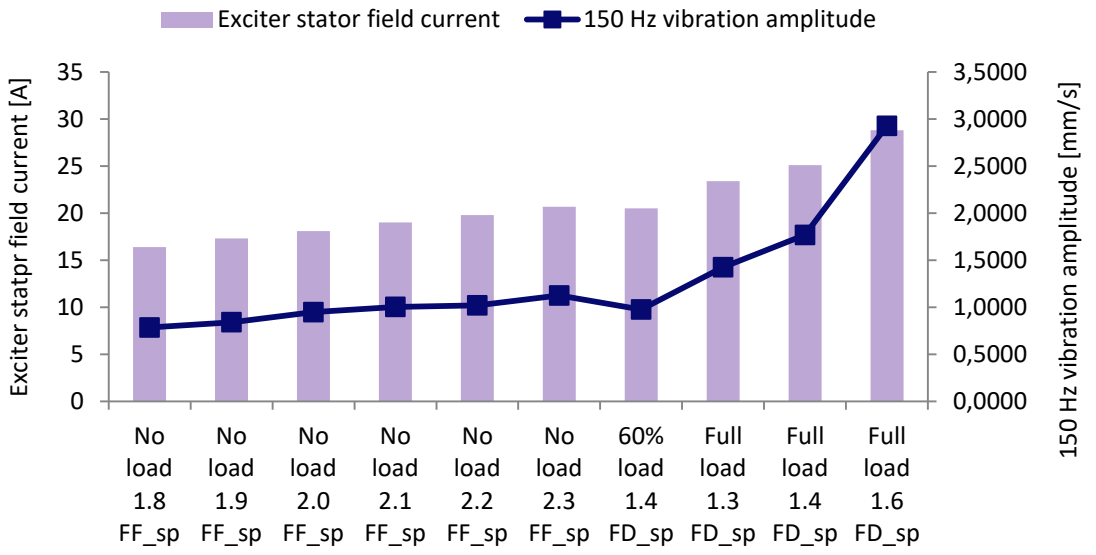

Figure 22. Exciter stator field current and observed amplitude of the –X tangential 150 Hz vibrations.

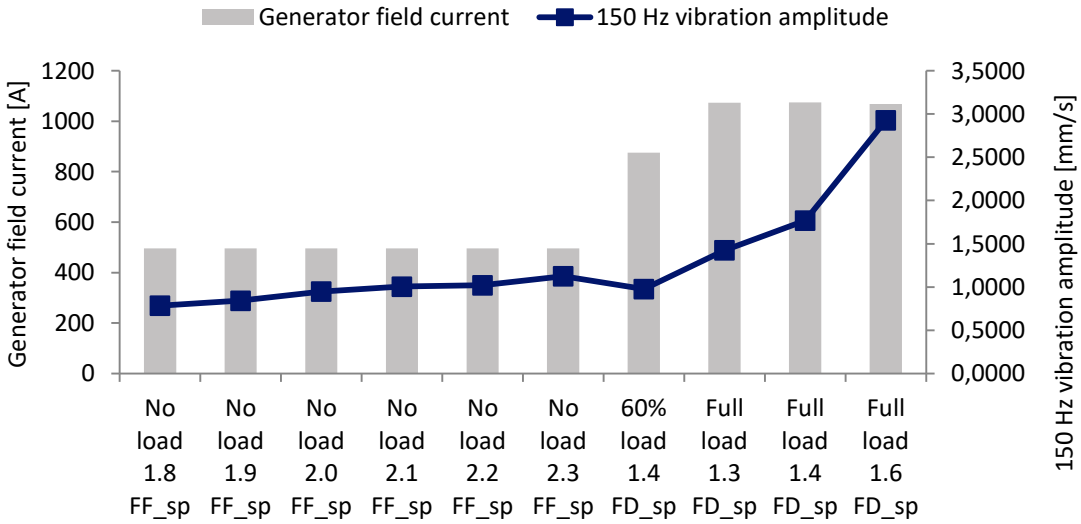

Figure 23. Generator field current and observed amplitude of the –X tangential 150 Hz vibrations.

5.2.1 Sensitivity analysis

All the vibration recordings contained 60 seconds worth of data. However, if studying the entire 60 seconds of vibrations, a smearing effect may take place making the results inaccurate. As mentioned before, a 4 second data segment, corresponding to 10 shaft rotations, was therefore used instead. To illustrate the impact of this smearing effect, Figure 24 shows the obtained –X tangential 150 Hz vibration amplitudes using a 4 second data segment compared to using all 60 seconds of vibration data.

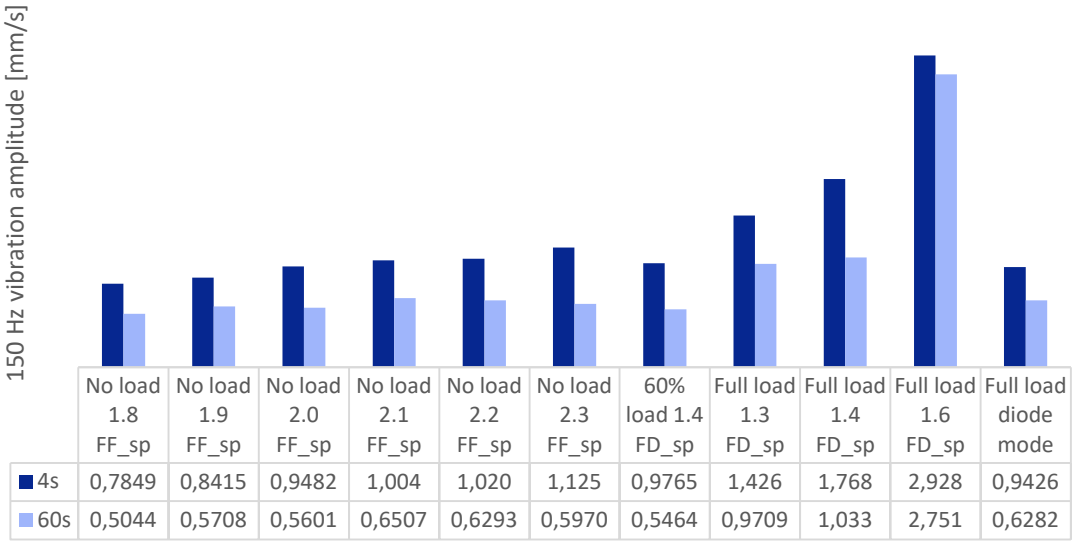

	No load 1.8 FF_sp	No load 1.9 FF_sp	No load 2.0 FF_sp	No load 2.1 FF_sp	No load 2.2 FF_sp	No load 2.3 FF_sp	60% load 1.4 FD_sp	Full load 1.3 FD_sp	Full load 1.4 FD_sp	Full load 1.6 FD_sp	Full load diode mode
4s	0,7849	0,8415	0,9482	1,004	1,020	1,125	0,9765	1,426	1,768	2,928	0,9426
60s	0,5044	0,5708	0,5601	0,6507	0,6293	0,5970	0,5464	0,9709	1,033	2,751	0,6282

Figure 24. Observed amplitude of 150 Hz vibration in the –X tangential direction for each setting. Comparison between 4s and 60s data segment.

As is seen in Figure 24, lower amplitudes are achieved when generating the spectra based on all 60 seconds of measurements instead of on a smaller segment. Also, the results in no load become unclear as an increase in firing angle no longer show an increase in vibration severity.

Since the analyzed 4 second segment of vibration data was arbitrarily chosen, a comparison between different choices of 4 second data segments, displayed in Figure 25, was also carried out.

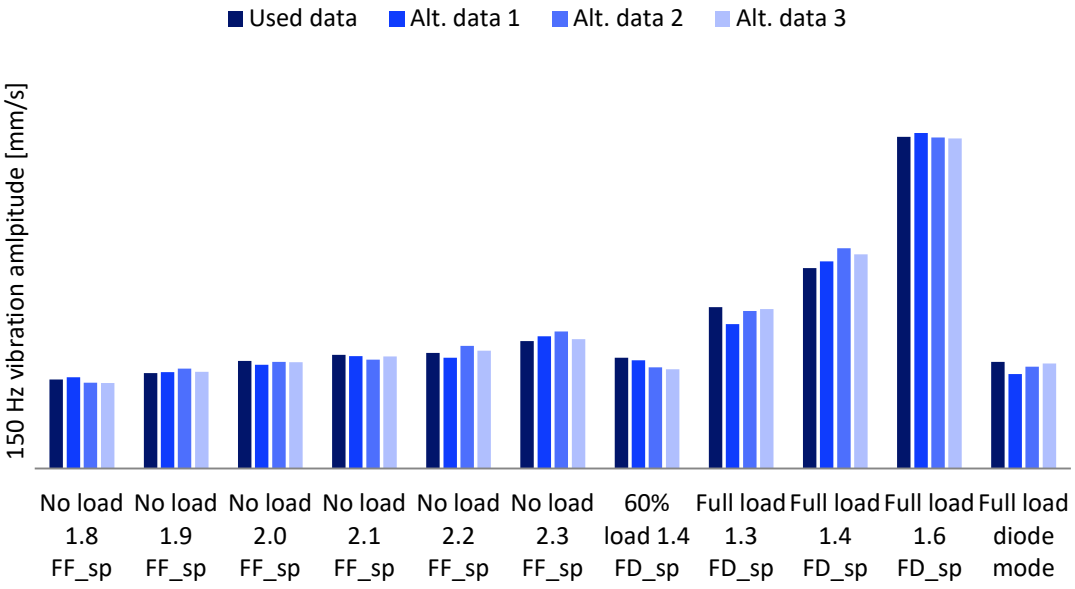

Figure 25. Observed amplitude of 150 Hz vibration in the –X tangential direction for each setting. Comparison between multiple 4s data segments.

It is visible in Figure 25 that the choice of 4 second data segment has little impact on vibration amplitudes. In addition to this, all data segments show the same trends regarding the interplay between firing angle and generator field current as did the studied segment. Hence, it appears that the choice of data segment is not of great importance as long as the chosen data segment is of appropriate length and does not contain any apparent disturbances.

Due to the distribution of the exciter stator poles, the accelerometers mounted on the stator frame in the –Y radial and tangential directions were placed right by a pole whereas the spacing of 90 degrees resulted in the corresponding –X accelerometers being placed at the space in between two poles. Figure 26 shows the 150 Hz vibration amplitudes measured in the –Y and –X tangential direction, where the underlying FFT was based on 4 seconds of vibration data.

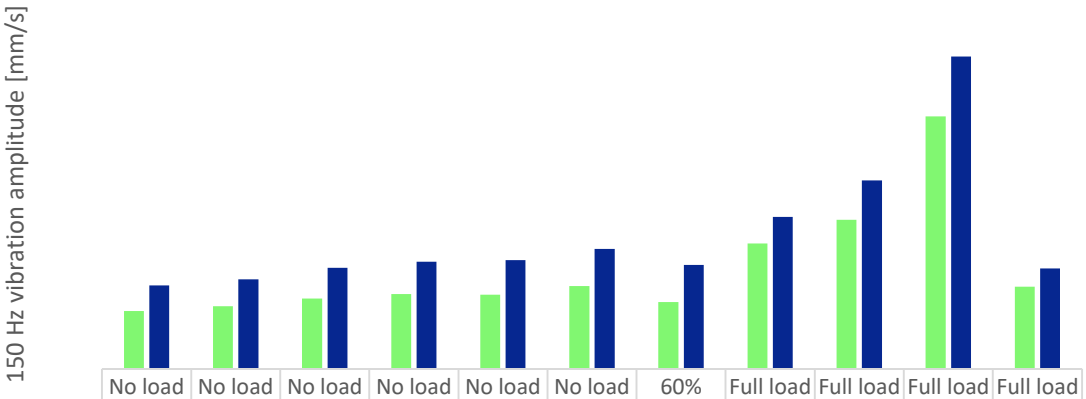

	No load 1.8 FF_sp	No load 1.9 FF_sp	No load 2.0 FF_sp	No load 2.1 FF_sp	No load 2.2 FF_sp	No load 2.3 FF_sp	60% load 1.4 FD_sp	Full load 1.3 FD_sp	Full load 1.4 FD_sp	Full load 1.6 FD_sp	Full load diode mode
-Y tan	0,5445	0,5881	0,6609	0,7033	0,6975	0,7764	0,6285	1,176	1,399	2,367	0,7715
-X tan	0,7849	0,8415	0,9482	1,004	1,020	1,125	0,9765	1,426	1,768	2,928	0,9426

Figure 26. Observed amplitude of 150 Hz vibration in the –Y tangential and –X tangential direction for each setting. Illustration of vibration amplitude variations with different placing of the accelerometers in relation to the exciter rotor poles.

Although the overall trend remains the same, it appears from Figure 26 that the placing of accelerometers in relation to the exciter stator poles does impact the amplitude of the recorded vibrations. Presumably, more damping is provided when placing the accelerometer by a pole than if the accelerometer is placed at the space in between poles. Hence, the accelerometer placing with regards to pole positions should be noted. It can however not be excluded that additional factors may have contributed to the difference between the –Y and -X tangential measurements.

5.3 Evaluation of vibrations

The observed vibration levels were evaluated from two perspectives. First, fulfillment of the NGTR and of ISO requirements was checked. Then, the observed exciter stator vibrations were compared to the known tangential eigenfrequencies.

5.3.1 Fulfillment of requirements

The requirement stated in NGTR is that the RMS value of the generator stator core vibrations are not to exceed 2.0 mm/s in any direction for any frequency. In this case the recorded vibrations were instead measured on the stator frame of a FRBE. Table 10 shows the fulfillment of the NGTR, when directly translated to the exciter, for the studied load cases.

Table 10. Fulfillment of the NGTR for the studied load cases.

Load case	Unfiltered signal	Filtered signal (FFT)
No load 1.8 FF_sp	NGTR fulfilled	NGTR fulfilled
No load 1.9 FF_sp	NGTR fulfilled	NGTR fulfilled
No load 2.0 FF_sp	NGTR fulfilled	NGTR fulfilled
No load 2.1 FF_sp	NGTR fulfilled	NGTR fulfilled
No load 2.2 FF_sp	NGTR fulfilled	NGTR fulfilled
No load 2.3 FF_sp	NGTR fulfilled	NGTR fulfilled
60% load 1.4 FD_sp	NGTR fulfilled	NGTR fulfilled
Full load 1.3 FD_sp	2.0 mm/s exceeded in tangential –Y and –X directions	NGTR fulfilled
Full load 1.4 FD_sp	2.0 mm/s exceeded in tangential –Y and –X directions	NGTR fulfilled
Full load 1.6 FD_sp	2.0 mm/s exceeded in tangential –Y and –X directions	2.0 mm/s exceeded in tangential –Y and –X directions at 150 Hz
Full load, diode mode	NGTR fulfilled	NGTR fulfilled

As is seen in Table 10, RMS values exceeding 2.0 mm/s were observed in the unfiltered vibration signals recorded in full load, thyristor mode. As the limit was exceeded in the tangential directions, the NGTR is not satisfied for those cases. For the FFT-filtered signals (see Figure 13 to Figure 20) the NGTR is fulfilled for all cases except for in full load, thyristor mode with the dynamic exciter field current set point set to 1.6. Here too the limit of 2.0 mm/s is exceeded in the –Y and –X tangential directions. All load cases do however satisfy the NGTR in the radial directions both for the filtered and unfiltered vibration signals.

Although the NGTR is commonly used when assessing generator vibrations, it is worth pointing out that not all generators are bound by the NGTR. Moreover, while the studied exciter may be a small, outer pole generator, the NGTR was developed for main generators rather than their excitation systems. Also, the construction year of the machines needs to be considered when evaluating the vibration levels. In this case, the studied exciter was constructed and installed before the currently valid edition of the NGTR was issued. In short, the relevance of the NGTR when evaluating exciter vibrations can be discussed.

Regarding the requirements on vibrations of bearing housings stated in ISO 20816-5: 2018, they are fulfilled at all times in full load thyristor mode. When comparing the vibration data displayed in Table 6 and Table 7 with the corresponding action limits presented in Table 2, it shows that even the most severe bearing housing vibrations registered are within acceptable levels. This since the action limit of A/B-C is never surpassed.

5.3.2 Eigenfrequencies and endurance

When comparing the vibration spectrums in Figure 13 to Figure 20 with the list of tangential eigenfrequencies in Table 8, the only tangential eigenfrequency for which a peak of significant amplitude is clearly visible in the vibration spectrums is that of 141.7 Hz, albeit in the radial directions. Nonetheless, as the frequencies 33.7 Hz and 47.6 Hz are found in the midst of some low amplitudes, it cannot be excluded that minor peaks exist also at these frequencies. Moreover, a peak of negligible amplitude can be seen around 209.8 Hz.

Based on what can be seen in the vibration spectrums, no tangential eigenfrequencies of the FRBE stator frame and machine top are triggered. Hence, the studied FRBE appears to have a safe design from this perspective. To ensure a safe design in terms of vibrations, it would also be necessary to investigate the radial and axial eigenfrequencies. Moreover, detailed analysis of the overall ability of the stator attachment to withstand vibrations should be carried out. This does however fall outside the scope of this thesis.

6. Conclusions

The main aim of this paper was to measure and analyze vibration levels on the stator of a FRBE, identify vibration origins and evaluate the observed vibrations in relation to existing standards and estimated eigenfrequencies. It has been noted that the vibration spectrums are primarily dominated by the peak at the first order electrical harmonic frequency, originating from rectification. During heavy load, this component has been observed to increase exponentially in amplitude with higher firing angles, similar to the expected behavior of the torque pulsations. Additional peaks of notable amplitude are found at the rotational frequency and the second and third order electrical harmonic frequencies. Minor contributions from the exciter rotor slots, the generator poles, the passing of the turbine blades and deviations in rotor roundness have also been detected.

When evaluated against generator vibration requirements, the observed, unfiltered vibration levels exceed the NGTR limit of 2.0 mm/s in the tangential directions for the runs in full load, thyristor mode. For all other cases, the NGTR is fulfilled in all directions. If instead evaluating the FFT-filtered vibration signals, the NGTR is fulfilled also for two of the three full load, thyristor mode cases. The ISO requirements on bearing housing vibrations are fulfilled at all times in full load, thyristor mode. Regarding the exciter stator eigenfrequencies, a peak is visible in the vibration spectrums at 141.7 Hz though not in the tangential directions. It appears that no vibrations of frequencies equal to any of the exciter stator tangential eigenfrequencies are triggered and so, from this perspective, the FRBE has a safe design.

As this is a case study, the conclusions are mainly limited to the studied system. In the broader picture this study does however support that the torque pulsations should remain the primary target for strategies aiming to mitigate FRBE stator vibrations. An alternative approach would be to optimize the mechanical design, focusing instead on the ability of the FRBE stator to withstand the vibrations it is subjected to. This approach is advantageous as it would not only target the vibrations due to rectification, but improve the overall endurance. Ideally, such an optimization of the mechanical design could then be extended to also include some of the mitigation strategies brought up in Chapter 2.

Finally, this study deserves criticism on a few remarks. As all vibration recordings were started manually at random times, the recordings have no common reference point in the exciter. By instead using a trigger to start the recordings, more detailed analysis could have been made regarding where in the exciter some vibrations come from, as vibrations of a certain frequency can have multiple sources. Also, the use of generator standards for the purpose of evaluating exciter vibrations, is not optimal. The basis of the NGTR, can be questioned as no information is provided on how the limit of 2.0 mm/s was decided upon. Regarding ISO, the location and small size of the exciter (see Figure 9) makes it likely that the main contribution to the bearing housing vibrations comes from the generator and the turbine.

6.1 Future work

A few focal points for future work are suggested based on the conclusions and limitations of this study:

- Simulations could be done, aiming to optimize the mechanical design of the FBRE with regards to its ability to withstand vibrations. Factors such as number of attachment points, stiffness and additional structures to improve the endurance could be considered. Taking it one step further, the implementation of some of the strategies for mitigating the air gap torque pulsations, brought up in Chapter 2, could also be included in the suggested FBRE design.

- Another option is to simulate the behavior of an FRBE with alternative approaches regarding the control of the rotating thyristor bridge rectifier to see if this could reduce the vibration levels.

References

[1] Brändström, F. Gustafsson, A. and Sjöström, L. (2016), “Vattenkraft”, Energimyndigheten, *http://www.energimyndigheten.se/forskning-och-innovation/forskning/fornybar-el/vattenkraft/* [Retrieved 2019-05-08].

[2] Schavemaker, P. and van der Sluis, L. (2008), ”Electrical Power System Essentials”, John Wiley & Sons Ltd. ISBN 978-0470-51027-8.

[3] Korsfeldt, T. (2011), “Vattenkraftens Roll i ett Hållbart Energisystem”, Svensk Energi, Stockholm.

[4] Byman, K. (2016), ”Sveriges Framtida Elproduktion, En Delrapport, IVA-Projektet Vägval El”, Kungl. Ingenjörsvetenskapsakademien, ISBN 978-91-7082-910-9.

[5] Nøland, J. K. (2017), “A New Paradigm for Large Brushless Hydrogenerators. Advantages Beyond the Static System”, Digital Comprehensive Summaries of Uppsala Dissertations from the Faculty of Science and Technology 1491, Uppsala: Acta Universitatis Upsaliensis. ISBN 978-91-554-9859-7.

[6] Nøland, J. K. et al. (2017), “Design and Characterization of a Rotating Brushless Outer Pole PM Exciter for a Synchronous Generator”, IEEE Transactions on Industry Applications, Vol. 53, No. 3.

[7] Nøland, J. K. (2018), “Unified Analysis and Modeling of the Dual-Control High-Speed Brushless Excitation System of Synchronous Generators”, IEEE Transactions on Industrial Electronics.

[8] Nøland, J. K. and Lundin. U, (2016), “Step Time Response Evaluation of Different Synchronous Generator Excitation Systems”, IEEE International Energy Conference, Energycon 2016-04.

[9] Nøland, J. K. (2013), “Electromagnetic Analysis of Rotating Permanent Magnet Exciters for Hydroelectric Generators”, Department of Energy and Environment, Division of Electric Power Engineering, Chalmers University of Technology, Göteborg.

[10] Nøland, J. K. (2016), “Fast-response Rotating Brushless Exciters for Improved Stability of Synchronous Generators”, Division of Electricity, Department of Engineering Sciences, Uppsala University, UURIE 347-16L, ISSN 0349-8352.

[11] Andersson, K. and Larsson, R. (2018), “Construction, Testing and Verification of a Brushless Excitation System With Wireless Control of the Field Current in a Synchronous Generator”, Uppsala University, UPTEC E 18 002, ISSN 1654 7616.

[12] Butros, P. (2011), “Simulations of Rotating Brushless AC Excitation System with Controlled Thyristor Bridge Rectifier for Hydropower Generators”, Uppsala University, UPTEC ES 11 024, ISSN 1650 8300.

[13] Torsteinsrud, O. (2018), “Education, Excitation Systems”, Voith Hydro, [PowerPoint-presentation], Unpublished.

[14] Nøland, J. K. et al. (2018), “Comparison of Thyristor Rectifier Configurations for a Six-Phase Rotating Brushless Outer Pole PM Exciter”, IEEE Transactions on Industrial Electronics, Vol. 65, No. 2.

[15] Nøland, J. K. Hjelmervik, K. B. and Lundin, U. (2016), “Comparison of Thyristor Controlled Rectification Topologies for a Six-phase Rotating Brushless Permanent Magnet Exciter”, IEEE Transactions on Energy Conversion, Vol. 31, No. 1.

[16] Wahlén, M. (2009), ”Bergeforsen G1 Borstlös Tyristormatare, Beräkning Luftgapsmoment”, R VGP/X 2009-125, VG Power AB, Unpublished.

[17] Biloš, J. and Bilošova, A. (2012), “Vibration Diagnostics”, Investments in Education Development.

[18] Taylor, J. I. (2003), “The Vibration Analysis Handbook: A Practical Guide for Solving Rotating Machinery Problems”, Ed. 2, Vibration Consultants, ISBN-10: 0964051729, ISBN-13: 978-0964051720.

[19] Statkraft and Vattenfall. (2018), “Nordic Generator Technical Requirements (NGTR)”, Rev. 6.

[20] Swedish Standards Institute. (2018), “Svensk Standard, SS ISO 20816-5:2018”, Available at *https://www.iso.org/home.html*.

[21] Wahlén, M. (2010), ”Jämförelse av Tangentiella Matarvibrationer BT-matare Kontra Diodmatare”, R VGP/X 2010-049, VG Power AB, Unpublished.